To the Graduate Council:

I am submitting herewith a thesis written by Richard Joel Thompson entitled "Computational Investigations of Characteristic Performance Improvements for Subkilogram Laser Micropropulsion." I have examined the final electronic copy of this thesis for form and content and recommend that it be accepted in partial fulfillment of the requirements for the degree of Master of Science, with a major in Mechanical Engineering.

Trevor M. Moeller, Major Professor

We have read this thesis
and recommend its acceptance:

Basil N. Antar

L. Montgomery Smith

Acceptance for the Council

Carolyn R. Hodges

Vice Provost and Dean of the Graduate School

COMPUTATIONAL INVESTIGATIONS OF CHARACTERISTIC PERFORMANCE IMPROVEMENTS FOR SUBKILOGRAM LASER MICROPROPULSION

A Thesis
Presented for the
Master of Science
Degree
The University of Tennessee, Knoxville

Richard Joel Thompson
December, 2009

Dedication

This thesis is dedicated to my parents, John Richardson Thompson and Lauren Michelle Thompson, to my sisters, Jennifer Michelle Heath and Jill Marie Thompson, and to my aunt, Nina Katherine Haile, for believing in me, inspiring me, and encouraging me to reach for new heights.

Acknowledgments

The author wishes to express his deepest gratitude to those who have assisted him throughout the development of this thesis, and to his school that has afforded him the opportunity to continue his education. Thanks is due to my advisor, Dr. Trevor Michael Moeller, for tirelessly putting up with my questions and helping me at every turn in the road. Thanks is also due to my committee, including Dr. Trevor Moeller, Dr. Basil Antar and Dr. L. Montgomery Smith, for their support and assistance in letting me achieve my degree; to Robert Rhodes, for his assistance in furthering my understanding of the Mach2 code and the Fortran language; to Nehemiah Joel Williams, for his valuable input regarding the nozzle construction for my simulations; to my fellow students here, Jason King, Nicholas Lister and Densu Aktas, for their support, encouragement and friendship; and, of course, to my family, who have always been there for me.

Abstract

Experimental investigations have evaluated the feasibility of using laser-driven plasma microthrusters for small-thrust, high-specific-impulse space maneuvers, particularly for micro- and nanosatellite missions. Recent work made use of the Mach2 hydromagnetics code for the construction of an adequate computational model of the micro-thruster operation. This thesis expounds on this previous work by extending the computational modeling capabilities, allowing for the determination of plasma plume properties and characteristic performance assessment of the microthruster; this allows for further computational investigation of the performance improvements achieved by new design considerations. Two particular design changes are implemented and measured: *(i)* the simulation of microthruster performance intentionally achieving laser-supported detonation of energetic polymer fuels for higher-thrust capabilities, and *(ii)* the implementation of an axisymmetric nozzle to improve passive solid-fuel performance. The Mach2 hydromagnetics code with the new performance assessment capabilities was used to examine the performance improvement of these new modes of operation; results of the simulations are presented and then evaluated for their use in the overall design of the plasma microthruster. Laser-supported detonation shows a tremendous potential increase in the laser momentum coupling coefficient C_m, and demonstrates a much higher thrust; the axisymmetric nozzle varies with nozzle half-angle and length, but still demonstrates expected nozzle trends and improves the laser momentum coupling coefficient, C_m, by up to 230% for some designs considered.

Contents

List of Tables

List of Figures

Nomenclature

η_{ab}	Ablation efficiency, defined as the ratio of ejected propellant kinetic energy to incident laser energy
β	Hall parameter
Δm	Ejected propellant mass during thrust
Δp	Change in momentum taking force constant
Δt	Total thrust time
Δv	Velocity increment achieved by thrust
Δw	Change in unit weight spacecraft propellant, taking force constant
$\dot{m}$	Mass flow rate of spacecraft propellant
η	First coefficient of viscosity
ρ	plasma mass density
σ	Electrical conductivity
$\bar{\bar{\boldsymbol{\tau}}}$	Fluid-dynamic viscous stress tensor
$\vec{\boldsymbol{B}}$	Magnetic induction vector field
$\vec{\boldsymbol{E}}$	Electric vector field
$\vec{\boldsymbol{j}}$	electric current density
$\vec{\boldsymbol{u}}$	Plasma velocity field

B^{α}	Contravariant components of the magnetic induction vector field
C_m	Laser momentum coupling coefficient
c_s	Speed of sound in a material
c_{s0}	Reference speed of sound in a material in the Mie-Gruneisen equation of state
F	Force
f	Boltzmann distribution function specifying number of particles in phase space volume element
$g^{\alpha\beta}$	Spatial metric tensor in contravariant components
g_0	Acceleration due to gravity, taken at sea level
I_{sp}	Specific impulse
m	Mass
$M^{\alpha\beta}$	Maxwell stress tensor
p	Linear momentum
p	Total fluid hydrostatic pressure
P_e	Electron fluid pressure
P_i	Ion fluid pressure
Q	Numerical forcing term introduced for stability reasons
q	Electric charge possessed by a particle
Q^*	Specific ablation energy of propellant
S_{coll}	Collision term in the Boltzmann equation, equal to change in number of particles occupying a phase space volume element
t	Time

v_{ex}	Average exhaust velocity of propellant ejected during thrust
W	Incident laser energy
w	Unit weight of spacecraft propellant
δ_{ij}	Kronecker delta, equivalent to the unit dyad
ϵ_0	Permittivity of free space
γ_0	Mie-Gruneisen equation-of-state
μ_0	Permeability of free space
Φ_{ei}	Electron-ion coupling term
ρ_0	Mie-Gruneisen equation-of-state reference density
ρ_e	plasma charge density

Chapter 1

Introduction

1.1 Overview and Purpose of this Thesis

This thesis aims to extend computational capabilities begun in previous work [2] for modeling laser-driven plasma microthrusters, allowing the determination of properties of the plasma plume emerging from the microthruster and characteristic performance assessment of the operation as a whole; this is done by extending the capabilities of the Mach2 hydromagnetics code to determine appropriate data for history output, and by introducing new data postprocessors that allow for the evaluation of the performance by considering well-known performance parameters such as thrust, laser momentum coupling coefficient, specific impulse, ablation efficiency, impulse bit and average exhaust velocity. The methodology developed in this thesis is then applied to two new modes of operation for performance evaluation. In one case, an energetic propellant is considered in lieu of the solid passive propellant used in previous computational [2] and experimental [3] investigations; in the second case, the performance improvement offered by the addition of an axisymmetric nozzle to the passive solid fuel is considered.

In this chapter, a brief explanation of the micro-thruster operation and a history of research in laser propulsion are presented. Chapter 2 focuses on the theoretical developments leading to a proper simulation of the plasma microthruster operation and describes the details of the Mach2 hydromagnetics code used. Chapter 3 presents the methodology by which the performance assessment and plume characteristics may be determined within the MACH2 code and the data postprocessors. Chapter 4 presents the construction of the energetic propellant computational model and the results from applying the developed methodology to the model; Chapter 5 presents the construction of an axisymmetric nozzle model for the solid-fuel microthruster operation and results achieved using applying the same methodology. Chapter 6 then examines the accomplishments made in this thesis and the results of the two simulations, followed by considerations of future work to extend these capabilities and results.

Laser propulsion has been extensively investigated [2, 4–6] for a variety of different applications. Launch vehicle designs have considered the use of ablative propulsion techniques and laser-supported combustion for achieving large-thrust missions (such as liftoff from earth) [4–7]; alternate designs have explored the use of ablative techniques for better-controlled, low-power-consumption altitude and trajectory adjustments [4]. Much has been performed in the way of experimental demonstration of proof-of-concept, measurements of attainable thrusts and specific impulse, and fuel investigations. New facilities have been constructed and dedicated to the research of improving laser propulsion options for higher-thrust missions [4].

With the recent interest in the development of micro- and nanosatellites, carrying mass restrictions of 100kg and 10kg respectively, new propulsion design challenges have been encountered. Current propulsion systems are not well-suited to the mission performance demanded by such mass restrictions, and often either require enormous power consumption or large fuel mass, both of which counteract the success of such a design. To this end, new investigations have been initiated in the last decade regarding the use of ablative laser propulsion for subkilogram propulsion system designs. This design has been demonstrated [3, 8] to achieve the necessary mission requirements for such satellites, and continuing studies have provided a range of options available for the application of such thruster designs for small-satellite missions [3].

While experimental demonstration has been actively pursued in recent years for the development of a subkilogram microthruster design, computational investigations of the thruster design have not been widely explored. An initial simulation of the plume expansion was performed [9] to explore the plume-induced contamination produced by the laser microthruster. More recently, research was pursued at the University of Tennessee Space

Institute by Dr. Trevor M. Moeller [2], investigating the development of a computational model of the microthruster operation with solid propellants. This work aims to continue these investigations by extending the existing computational model in order to investigate performance improvements introduced by a variety of design considerations.

A computational investigation of the laser microthruster design would be invaluable for the purposes of furthering theoretical understanding of the design parameters and for determining expected performance improvement due to design changes. This would reduce costs, time, complexity and uncertainty associated with an experimental investigation. A code capable of adequately modeling the physics associated with the laser-plasma interactions mediated in the transfer of energy from the laser to the propellant would provide a much faster, easier, and inexpensive means of investigating the physics associated with the laser microthruster design, and the performance improvements associated with different designs.

This thesis investigates the performance improvements offered by two predominant design considerations: *(i)* the introduction of an exothermic (explosive) propellant in lieu of the solid propellant modeled previously, and *(ii)* the addition of an axisymmetric nozzle to improve thermal expansions of the plasma plume in order to increase efficiency and thrust. Working computational models of each design consideration are demonstrated, and a methodology of examining performance parameters associated with the computational models is developed. These performance parameters are measured from the simulation results, and compared with existing experimental data and with the previous solid-propellant modeling performed [2]. A comparison of these results is then presented.

1.2 A Brief History of Laser Propulsion

It was only a matter of six years after the first demonstration of an operable laser that scientists and engineers posed the question of how such a device could be used in propulsion [10]. There is a strong variety of suggestions in answer to this question; laser propulsion tends to a wide diversity of optimal missions due to the extensive differences in how the laser may be applied. Applications have been found from single-stage-to-orbit flights to submillimeter stationkeeping thrusters. This makes the term 'laser propulsion' very broad and cannot be used to specify the precise nature in which the laser is being applied. Therefore, a variety of names appear in literature; the form of laser propulsion explored in this thesis corresponds to micropropulsion on a submillimeter, submillisecond scale.

The first concepts of using lasers for propulsion revolved around relativistic ideas for interstellar and interplanetary travel. These mostly consisted of theoretical ideas that could not be easily demonstrated [10]. Eugene Sänger proposed the idea of using photon rockets to create a blackbody drive, which would ride the momentum exchange of launching photons into free space; he could never successfully introduce a means to collimate and redirect the high-energy gamma rays. Newer ideas [10] have explored the use of an antimatter fuel to accomplish the same drive; however, although this concept was probably the earliest introduction of lasers to propulsion, it still remains the most unaccomplished in practical demonstration.

Light exhibits a finite momentum, energy and pressure; these quantities do not correspond exactly to the traditional sense applied to ordinary matter, but require some understanding of the quantum nature of light in order to quantify. However, the visible overall presence of light's pressure may also be harnessed for space exploration by the use of large solar sails. Extensive investigations have been made for such sails [4], but they also still require practicality in demonstration. Solar sails are advantageous in that they do not carry any fuel, but require very indirect paths of movement and very large lasers for movement.

Kantrowitz [4] was the first to suggest using the laser in an indirect manner to ablate the propellant, rather than either combusting the propellant by chemical means or relying purely on relativistic interactions with light. This deceptively simple idea may seem at first glance as only a minor improvement to the method of initiating the combustion; however, due to the interactions between the laser light and the propellant, by using such a method we gain access to an extensively different domain of physics. The focusing of a laser beam onto a propellant can heat the propellant into a plasma, in which very different interactions occur between the light and matter. This leads to very different theoretical results concerning the use of lasers in propulsion, which are not subject to the famous chemical limitations of rocketry [11].

The idea of ablating the propellant with a laser still applies to a wide variety of propellant, spacecraft and sizes. The Myrabo lightcraft idea [7] lends more to the application of a ground-based or space-based laser used for ablating a large mass to deliver a payload from the ground to orbit. This requires a laser with significant power and intensity, and laser attentuation may occur between the laser and the target ablation mass. The Myrabo lightcraft can achieve on the order of 900N/MW experimentally at the state of the art; however, much more investigation and demonstration is needed before such a system will be considered adequate for any mission.

1.3 Subkilogram Laser Micropropulsion

Subkilogram laser micropropulsion is a more recent innovation in design for the application of the ablation of propellants to microsatellites and nanosatellites, which exhibit total orbiting mass restrictions of 100kg and 10kg, respectively. Recent trends in satellite design have begun pursuing the development of such satellites because of the benefits of reduced costs for launch, total satellite construction, and less complexity in the overall system. Micro- and nanosatellites present an abundance of design challenges, but perhaps the most important design consideration is an adequate propulsion system suitable for micro- and nanosatellite missions. Such mass restrictions demand a propulsion system that exhibits long lifetime for both the operable device and available fuel, simplicity in design, high efficiency, low power consumption and low additional fuel mass requirements. To this end, a propulsion system suitable for an operable 100kg or 10kg mass restriction would be termed *subkilogram*. Since a satellite nominally requires six such thrusters for full-degree operation, any suitable propulsion device must probably be at least less than a kilogram in total mass.

While it is the goal of any well-designed propulsion system to meet the above listed qualities, no current propulsion system would be particularly adept for any micro- or nanosatellite mission. Chemical techniques are clearly insufficient for propulsion aboard any such satellite, due to low efficiencies and large additional fuel mass requirements; furthermore, chemical propulsion systems are grossly complex and do not fulfill the range of performance requirements necessary. Electric propulsion systems including the typical variety (ion thrusters, Hall thrusters, magnetoplasmadynamic thrusters, etc.) are also not well-suited to such a mission requirement, due to the large power consumption of such devices and intricate design.

Recent proposals [3] have investigated the idea of applying the laser ablation of a solid propellant to subkilogram satellite propulsion. Initial experimental investigations were very successful at demonstrating the thruster requirements needed for such a thruster [8]. Requirements for such a design that might be considered a commercial prototype of a μLPT are quoted in Table 1.1 [1]. The proposed design of the micro-laser ablation thruster (μLPT) incorporates a diode laser and a tape strip in a configuration as presented in Figure 1.1. Two primary modes of operation have been explored; in the first, called *reflective mode*, the laser is angled to ablate the upper surface of the solid propellant. Reflective mode is capable of achieving the highest thrusts and coupling coefficients, but unfortunately exposes the optics to the plasma plume, which contaminates and degrades the thruster very quickly. A new mode termed *transmission mode* was alternately investigated after early experiments, wherein the laser is focused onto the bottom of the propellant tape from underneath, with a transparent substrate layer mediating the laser energy while protecting the thruster optics; the transmission mode has been adopted for a commercial design of the μLPT [1, 12–15]. Newer commercial prototypes have incorporated up to eighteen fiber lasers at average powers of 100W each to provide ablation [16]. The transmission-mode laser micro-thruster concept design is shown in Figure 1.2.

More recent experiments [1, 14, 15] have investigated the application of liquid polymer propellants with exothermicity, which exhibit explosive properties due to additional chemical energy stored in the propellant. The realized improvement in performance of the μLPT operation with the new energetic propellant is significant enough that an alternate μLPT design has emerged; the previous thruster is now called the nsμLPT and the new termed the msμLPT; the former aims to achieve maximum specific impulse and fuel economy, while the latter achieves higher thrust and coupling coefficient. Even more recent literature [16] suggests combining multiple modes of operation into a single propulsion unit, since the only difference in design is essentially the laser intensity on the target propellant. Interest has also been expressed in the same literature in achieving a 6-N-capable subkilogram laser plasma micro-thruster.

Table 1.1: Characteristic commercial subkilogram laser plasma micro-thruster (μLPT) design parameters. [1]

Design Parameter	**Normal Thrust**	**Max Thrust**
Laser Sequence	Sequential	Parallel
Laser Average Power, [mW]	45	4.54
Laser Repetition Frequency, [Hz]	1.89	63
Operating Lifetime, [hrs]	44	1.1
Avg. Power Input [W]	2.0	18.3
System Coupling Coefficient, [N/MW]	50	550
Tape Coating Material	Glycidyal Azide + Carbon	
Tape Thickness	140	
Ablatable mass, [g]	44	
Tape length, [m]	30	
Tape width, [mm]	8	
Type of Laser	JDSU 6390	
Laser Peak Power, [W]	8	
Laser Pulse Duration, [ms]	1.5	
Coupling Coefficient, [N/MW]	2200	
Specific Impulse, [s]	250	
Focal Spot, [L $\times$ w, μm]	1333$\times$40	
Number of Lasers	6	
Lifetime Impulse, [Ns]	48	
Mass, [kg]	0.54	

1.4 Investigations Made in this Thesis

In light of the recent interest in improving and refining the design of the μLPT, it is of considerable interest to develop a working computational model that may be used to investigate the physics and design influences of the micro-thruster operation. Previous computational work [2] has already indicated that such a model can be constructed. This thesis continues the previous work in an effort to develop new computational models of the μLPT in operation with different design concepts introduced. By comparing the new designs investigated here with previous experimental work and the baseline tests presented in [2], demonstration of significant micro-thruster operation improvement may be demonstrated.

A methodology is developed and detailed in Chapter 3 of this thesis, explaining how

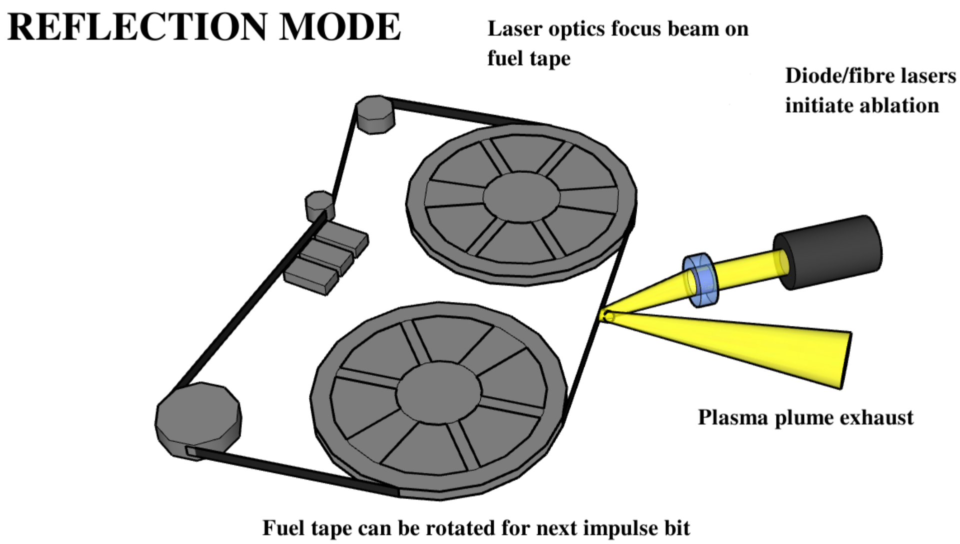

Figure 1.1: Design concept for micro-thruster operation in reflection mode.

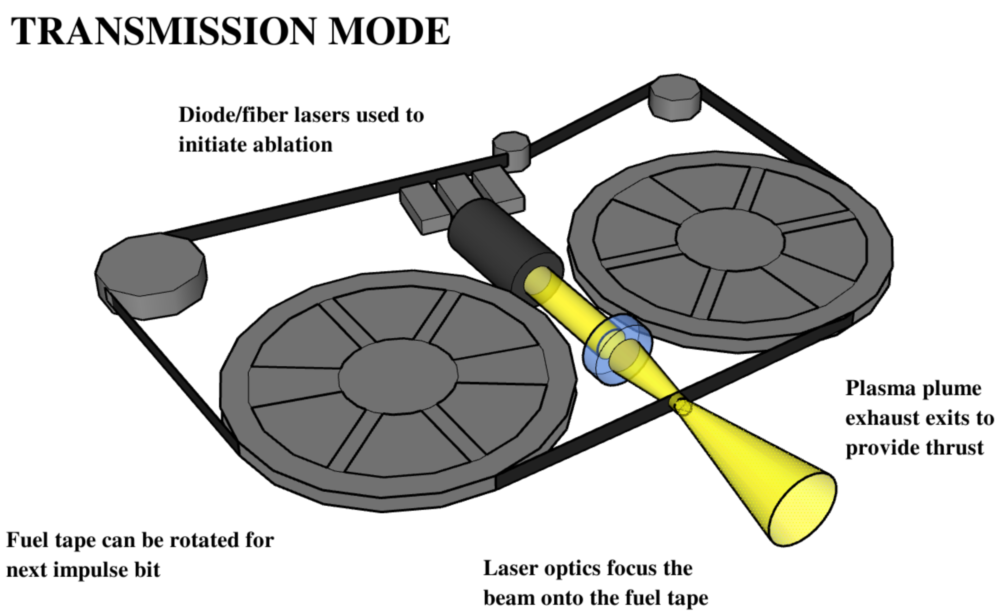

Figure 1.2: Design concept for micro-thruster operation in transmission mode.

the computational methods investigated here characterized the performance of the microthruster. This partially involved characterizing the plasma plume. The MACH2 code (which is explained in greater detail in Section 2.3) is a hydromagnetics code capable of simulating the laser ablation and plasma plume expansion, and the MACH2 history routine that writes output data was modified to allow for diagnostics on the microthruster operation and plasma plume characterization. This data was then postprocessed by external software, written for the purpose of this thesis; the ejected mass and thrust were taken as primary determinations, and other characteristic performance parameters, including specific impulse and laser momentum coupling coefficient, were determined from these measurements in the postprocessing software. The capabilities introduced in the MACH2 code and in the postprocessors assume that the input file was written specifically for an Eulerian frame of reference attached to the spacecraft. Following the development of the methodology for evaluation of the performance, this methodology was applied to the two cases of changing the propellant to an energetic material and adding an axisymmetric nozzle.

Due to the recent interest in developing a 6-N-capable subkilogram system, a different method of implementing the energetic propellant is simulated in which the propellant is intentionally detonated in a new fuel tape design consisting of 'rings' filled with exothermic fuel. Such a design would allow for single-shot operation of the thruster with much larger thrusts than previous experimental work achieves; further, the design implementation in a commercial model would require the use of higher laser intensities; this may be achieved by using shorter pulse durations (on the order of microseconds to nanoseconds), which has already been demonstrated in working commercial prototypes [1]. Chapter 4 of this thesis investigates a computational model of the energetic propellant; the achievement of laser-supported detonation simulated in this thesis effectively raised the coupling coefficient by an order of magnitude over the previous computational work for the same laser settings, and also demonstrated an increase by two orders of magnitude over the experimental data in which the same fuel was used, but detonation was not achieved.

In the interest of finding new design enhancements that do not require fuel tape modification or that still retain the use of passive solid targets, axisymmetric nozzle designs were introduced and simulated. Chapter 5 of this thesis discusses a computational model of the micro-thruster with attached solid nozzles that would be machined or fabricated by deposition techniques, and briefly investigates the design parameters of half-angle and length influencing the performance of the micro-thruster. Comparisons to available experimental trends confirm that an axisymmetric nozzle added to the microthruster improves performance by raising the ablation efficiency, coupling coefficient and specific impulse over that of the computational baseline and previous experimental data. An optimal nozzle configuration was not explored in this thesis, only the demonstration that such trends can be shown and confirmed.

It is hoped that the work performed here will influence future design considerations of subkilogram laser micropropulsion devices by demonstrating the use and implementation of new design concepts and by providing base computational work that may be built off of and expanded for future needs. Alternate design considerations that could equally be investigated with the computational abilities demonstrated here are examined briefly at the end of this thesis, including the idea of a magnetic nozzle design that would improve the movement of the plasma plume away from the spacecraft.

Chapter 2

Theoretical Foundations

2.1 Characteristic Performance Parameters

Thrusters and propulsion devices are essentially designed to produce a force by an exchange of energy or momentum as efficiently as possible. The device design is not restricted to any one mode of operation; therefore, many different approaches are available for development as a means of producing a force. However, despite a variety of available techniques for achieving thrust, it is still desirable to compare these thrusters to determine which technique is most appropriate for any given mission. These comparisons may be made by determining certain characteristic performance parameters, which evaluate the most important aspects of the thruster's functionality. It is the concern of these parameters to validate any claim of advantage of one specific thruster design over another.

The performance parameters most commonly explored in propulsion systems include the specific impulse, overall propulsion system efficiency, thrust, fuel-to-mass ratio, mass fraction for any particular mission, and lifetime of the thruster and/or thruster fuel. Some of these parameters are characteristic of the spacecraft, including fuel-to-mass ratio and mass fractions. These will not be explored in this thesis, since we are interested primarily in the development of an independent propulsion system. Differences arise in the physical interpretation of certain parameters and their importance due to the physics of how the thruster operates. For example, the mass of the fuel is not nearly as significant for an electric propulsion system as the mass of the power plant [17]. In addition, laser propulsion features some of its own performance parameters that do not have analogues to other forms of propulsion. These characteristic performance parameters will be explored and defined below and then used as defined throughout the remainder of the document. A description of the details regarding the MACH2 code is presented subsequently, and Chapter 3 focuses on the calculation of performance parameters in the context of the MACH2 code and its output data.

Specific impulse, denoted I_{sp}, is defined physically as the impulse imparted to the spacecraft per unit weight of propellant, $\frac{dp}{dw}$ [17]. This may be considered as a conversion factor between the weight amount of propellant burned and the corresponding impulse imparted to the spacecraft. Mathematically, it is linearly related to the exhaust velocity of the burned propellant out of the spacecraft. This may be written via several relations [18]:

$$I_{sp} = \int_0^t \frac{dp}{dw} dt = \int_0^t \frac{dp}{dt}\frac{dt}{dw} dt = \frac{\int_0^t \frac{dp}{dt} dt}{\int_0^t \frac{dw}{dt} dt} = \frac{\int_0^t dp}{\int_0^t dw} = \frac{\int_0^t F dt}{\int_0^t g\dot{m} dt} \tag{2.1}$$

For solid propellants, the thrust and propellant consumption vary over the period of the burn, and the above integral form must be used. However, for liquid propellants, the thrust and flow rates may often be considered constant [18]. In these cases, the specific impulse reduces to

$$I_{sp} = \int_0^t \frac{dp}{dw} dt = \frac{\int_0^t dp}{\int_0^t dw} = \frac{\Delta p}{\Delta w} = \frac{\Delta p}{\Delta t}\frac{\Delta t}{\Delta w} = \Delta m \frac{\Delta v}{\Delta t}\frac{1}{g}\frac{\Delta t}{\Delta m} = \frac{\Delta v}{g_0} \tag{2.2}$$

In the rest frame of the spacecraft, this Δv represents the change in velocity achieved by the ejected propellant, which is the exhaust velocity, v_{ex},

$$I_{sp} = \frac{v_{ex}}{g} \tag{2.3}$$

thus demonstrating the comment above that the specific impulse is related linearly to the exhaust velocity. The simulations in this thesis will explore the improvement of specific impulse extensively for the proposed alternative design considerations.

The *laser momentum coupling coefficient*, C_m, is an important parameter describing the effective energy transfer mechanism between the laser and the propellant. It may be physically considered as the number of units of impulse generated by a single unit of incident laser energy, $\frac{dp}{dW}$ [3]. In this sense, it acts as a conversion factor between the incident laser energy supplied to ablate the propellant and the resulting impulse released. It may also be physically considered as a conversion between the laser power deposited during the ablation process, and the resulting thrust provided by the plasma plume [8]. It is intimately related to the specific ablation energy, Q^*, which describes the amount of energy absorbed by the material to ablate a unit mass of the propellant, $\frac{dW}{dm}$ [3]. These two parameters are related via their product,

$$C_m Q^* = \frac{dp}{dW}\frac{dW}{dm} = \frac{d}{dm}(p) = \frac{d}{dm}(mv) = 1 \cdot v|_a^b \tag{2.4}$$

which is again, in the reference frame of the spacecraft, the change in velocity achieved by the ablated propellant. This corresponds to the exhaust velocity, v_{ex}. Hence, from the above relation for the specific impulse I_{sp}, it is realized that the specific impulse and laser momentum coupling coefficient are not arbitrary, [3]

$$\frac{I_{sp}}{C_m} = \frac{Q^*}{g} \tag{2.5}$$

It is clear that these significant parameters are dependent on each other, and cannot simply be increased or decreased arbitrarily.

It is not always in the best interest of the thruster to simply increase either the coupling coefficient C_m or the specific impulse I_{sp} without bound. The requirement of C_m and I_{sp} is mission-specific, and there exists an optimal arrangement per mission. Unduly high parameters can also impact other design parameters; for example, the propellant fuel lifetime decreases very rapidly with increasing coupling coefficient C_m [3]. A clear indication of the uselessness of unboundedly large cases may be seen if we take the two opposite case limits. If we increase the coupling coefficient without bound, we have

$$\text{Infinite-thrust engine} = \begin{cases} C_m = \frac{dp}{dW} \to \infty \\ I_{sp} = \frac{dp}{dw} \to 0 \end{cases} \tag{2.6}$$

Clearly, in such a situation we will have an enormous thrust, but the C_m is so large that the fuel is completely depleted before the mission is complete. In contro, we could design an opposite such limit,

$$\text{Infinite-fuel engine} = \begin{cases} C_m = \frac{dp}{dW} \to 0 \\ I_{sp} = \frac{dp}{dw} \to \infty \end{cases} \quad (2.7)$$

In this case, an unduly high I_{sp} conserves the fuel indefinitely, but the engine provides no thrust [3].

Since we cannot use an engine with no thrust or no fuel, we must find a compromise and determine an optimal arrangement such that a necessary thrust is produced without depleting all of the fuel. Such an optimum must be determined for any given mission before any design parameters may be established.

Efficiency is an important evaulation in any engineering application. The efficiency is the ratio of output energy to input energy. There are a variety of efficiencies to be examined on any complex spacecraft system. This thesis is not interested in the overall design of the entire spacecraft; therefore, these efficiencies do not concern the investigations made here. The most important efficiency in a laser propulsion system is the *ablation efficiency*, η_{ab}, defined as the ratio of the kinetic energy of the resulting propellant ejection from a single pulse to the incident energy on the target propellant from the laser,

$$\eta_{ab} = \frac{(\text{Kinetic energy of ejected propellant, } E_k)}{(\text{Incident Laser Energy, } W)} \quad (2.8)$$

Traditionally, efficiencies take forms less than unity; however, it is important to note that if an exothermic reaction occurs in the ablation process (for example, if the propellant initiates a detonation that releases substantial chemical energy), the ablation efficiency, by its explicit definition, may be much greater than unity. For passive materials for which no chemical reactions take place, like the polyvinylchloride polymer propellant investigated previously [2, 8], the ablation efficiency must be less than unity. Ablation efficiencies much larger than unity will be demonstrated in the computational simulations performed here in Chapter 4, where energetic propellants will be explored. In the other simulations presented here, ablation efficiencies will be much less than unity, indicating the loss of energy due to transfer mechanisms involved in the laser-plasma interactions. The investigations in this thesis will consider the ablation efficiency extensively, since this indicates the overall success of the energy transfer mechanism from the laser to the propellant ejection.

The ablation efficiency η_{ab} may be expressed in terms of the coupling coefficient and specific impulse. If we write η_{ab} in terms of the mass ejected Δm and average exhaust velocity v_{ex}, [3]

$$\eta_{ab} = \frac{\Delta m v_{ex}^2}{2W} = \frac{1}{2}{C_m}^2 Q^* = \frac{1}{2} g_0 C_m I_{sp} = \frac{1}{2} C_m v_{ex} \tag{2.9}$$

Hence, the ablation efficiency is also coupled to the system of performance parameters.

An important indication of the available I_{sp} for laser propulsion missions is revealed if we require the propellant be passive, ie., no exothermic reactions occur, so no additional chemical energy is released. In such a case, only incident laser energy may be transformed into mechanical energy of the ejected propellant, and so the ablation efficiency η_{ab} must be less than unity. In such a case, we have an inequality concerning the relation of the specific impulse and coupling coefficient from the above relation,

$$\eta_{ab} \leq 1 \text{(for passive target propellants):}$$

$$C_m I_{sp} \leq \frac{2}{g_0} \approx 0.204 \left[\frac{\text{sec}^2}{\text{m}}\right] \tag{2.10}$$

This establishes a calculable limit to the attainable specific impulse for micro-laser-propelled vehicles. For a comparison, chemical rockets demonstrate a theoretical upper limit of approximately 500s due to temperature limitations of the flow. The space shuttle's main engine attains a practical value of 465s. Since this limit is fundamental, it cannot change by introducing new propellant materials; it a limitation to the form of propulsion used. Electric propulsion demonstrates no theoretical limit to attainable I_{sp}, but the energy requirement for the mission scales with I_{sp} [17]. However, laser propulsion has demonstrated coupling coefficients on the order of 1,000N/MW; furthermore, the ablation efficiency has been demonstrated [3] to approach 100%. This yields a very high attainable specific impulse. Experimentally, laser propulsion has been demonstrated to exhibit up to 7,600s of I_{sp} with 20ns-duration pulses from typical KrF lasers illuminating aluminum targets [1]. In more recent experimental demonstrations of the microthruster, measurements of passive gold targets ablated with the microthruster achieved a measured 95% ablation efficiency and over 3,600s of I_{sp} [16]. This level of specific impulse competes with the most recent magnetoplasmadynamic thruster measurements and NASA's HIV-HAC Hall thruster. [3] It is believed [3] that 10ks of I_{sp} is possible experimentally.

In the case of exothermic propellants, the ablation of the target propellant releases additional chemical energy that contributes to the kinetic energy achieved by the ejected propellant. This allows the possibility for the ablation efficiency to be much greater than unity. In practice, however, this does not often occur; recall that the performance parameters are dependent. The introduction of the exothermic reactions largely increases the thrust and C_m, which limits the available I_{sp}. From a point of view of thruster and propellant selection, an exothermic propellant provides a large C_m, low I_{sp} option for higher-thrust missions, while the passive targets tend to provide a much higher I_{sp} and low-thrust option.

Thrust is the essential product of any propulsion system. It is an important consideration for mission specifications, because producing an unnecessary amount of thrust is a waste of the limited resources available on a spacecraft, while a thrust not large enough to perform the necessary mission is a wasted mission. Thrusts can vary widely for missions; spacecraft attempting to achieve escape velocity from the surface of a planet will typically need an enormous force, while most missions occuring in space typically need characteristically low thrust, particularly for attitude and orbit trajectory adjustments and stationkeeping.

The rocket equation results from Newton's second law when mass is considered a time-dependent quantity,

$$F_t = \frac{dp}{dt} = \frac{d}{dt}\left(mv)\right) = \frac{dm}{dt}v + m\frac{dv}{dt} \tag{2.11}$$

Typically, the second term does not contribute significantly to the measured force, so this term is dropped. In such a case, we end up with an expression for the rocket thrust generated by the mass flow rate and exhaust velocity of flow,

$$F_t = \dot{m}v_{ex} \tag{2.12}$$

Clearly, higher mass flow rates or higher exhaust velocities will achieve a higher thrust.

In most applications, higher mass flow rates are not practical, due to the scaling of extra fuel that must be carried for flight. Most rocket engines aim to achieve higher exhaust velocities in order to increase the thrust.

There is a characteristic gulf between chemical and electric propulsion systems in typical thrusts; chemical rockets can generate meganewtons of thrust, while electric propulsion devices typically achieve between micronewtons and millinewtons. This means chemical rockets provide a good high-thrust, low-I_{sp} option, while electric propulsion serves for good low-thrust, high-I_{sp} missions. Laser propulsion fills the gap between these two, providing a large variation of mission options itself. Ablative laser propulsion for launch vehicles has achieved a C_m as high as 900N/MW, indicating a thrust of 900N per megawatt delivered by the laser. [4] This was performed for a laser-detonated solid propellant, designed for small payload launch. On the other extreme, subkilogram propulsion systems have achieved measured thrusts between micronewtons and tens of millinewtons [16]. The simulations presented in this thesis confirm the latter thrust for the commercial design, and enhance the thrust by the introduction of new design considerations.

Thruster lifetime is an important consideration for the length of time the thruster will be in an operable condition. Laser propulsion systems are usually most limited in lifetime by the optics of the system or by the fuel lifetime. Several laser propulsion systems have suffered significant and frequent damage to the optics of the thruster, which destroys the usefulness of the thruster completely. The *transmission mode* capability for the subkilogram laser plasma microthruster tends to eliminate this problem due to the optically transparent substrate. The thruster lifetime will not be considered in this thesis, since it is difficult in these simulations to quantify the state of the optics, and a simulation would not justify a lifetime estimate for a commercial model. We mention this here because the contamination of the optics by a plasma plume could be considered in future work; previous simulations have attempted such a quantification [9].

2.2 Laser-Plasma Interactions and Laser-Sustained Plasmas

A comprehensive understanding of the physics of interation between the laser and the propellant is prerequisite to any indepth study of a propulsion device driven by such a mechanism. The physics of plasma interactions are governed by the equations of fluid mechanics and electrodynamics; the interaction with the surface of the solid and ablated propellant depends predominantly on heating and inverse *bremsstrahlung* processes. The absorption of light by the plasma is strongly dependent on the collisionality of the plasma, as noncollisional motion does not contribute to the absorption or emission of light. Mathematical closure of the fluid and electrodynamic equations must also be demonstrated before any solution may be sought. Sufficient initial and boundary conditions must be further specified to elicit any solution to these equations. Furthermore, design considerations of the propulsion system must take into account the physics presented here and previous experimental work investigating the practicality of using this transfer mechanism for providing thrust. It should be remembered throughout this section that laser-plasma interactions are very complex, and hence there are components of the theory still not fully understood [19].

A plasma is a gas in which sufficient heat has been provided through various means to strip the electrons from their orbits around electrically-neutral atoms. This results in a 'soup' of electrically-charged particles and electrically-neutral particles. The simplest form of a plasma would be a gas consisting of three species: positively-charged ions resulting from singly-ionized neutrals, negatively-charged free electrons stripped from orbits, and remaining neutral atoms. Doubly-ionized particles, recombinants and other constituents introduced by complex interaction phenomena may occur, making plasmas typically much more complex than this simple model. Since plasmas tend to exhibit quasi-neutrality of charge over large time and length scales, the number densities of each species is usually coupled by the free electron number density, n_e.

Plasmas are characterized by a number of parameters. Number densities of different species present in the plasma is one characterization. The electron, ion and neutral atom temperatures, T_e, T_i, T_n respectively, also determine the physical phenomena occurring in the plasma interactions. The electron Debye length, λ_D, physically describes the shielding length within which quasi-neutrality breaks down. Plasmas are typically of characteristic length scales much larger than the Debye length λ_D, which enforces quasi-neutrality. The electron Langmuir frequency (also commonly called the electron plasma frequency), ω_p, dominates the transport properties exhibited by the plasma; as an inverse, this quantity may be considered the time scale of charge separation. Degree of ionization, α, is also crucial to determining what physical phenomena may result within the plasma; the response of weakly-ionized plasma is much different from the response of fully-ionized plasma.

Since plasmas are ionized gases, the fluid dynamic equations corresponding to compressible, viscous gases adequately describe the motion of the plasma. If we consider the N particles in a gas to span a phase space of 6^N dimensions, representing the three spatial and three velocity components, then there exists some distribution function f which specifies the number of particles in a phase space volume element $d\vec{\boldsymbol{r}}d\vec{\boldsymbol{u}} = dxdydzdudvdw$. The change of the number of particles in a volume element may only occur through changes via collisions with other particles, so

$$\frac{df}{dt} = S_{coll} \tag{2.13}$$

where S_{coll} represents the change of particles in any volume element; this must be represented by a collision model which must be introduced separately; however, since we are interested in the general equations describing the fluid as a whole, we sum over all species of particles in the distribution, which integrates out the collision term, so we will avoid discussing it here in much depth.

Applying the chain rule of differentiation to the distribution function, which is an explicit function of time, position and velocity, we have

$$\frac{df}{dt} = \frac{\partial f}{\partial t} + \frac{\partial f}{\partial \vec{\boldsymbol{r}}}\frac{d\vec{\boldsymbol{r}}}{dt} + \frac{\partial f}{\partial \vec{\boldsymbol{u}}}\frac{d\vec{\boldsymbol{u}}}{dt} \tag{2.14}$$

But we identify the acceleration and velocity in the above expression, and equate these to the collision term. Due to the strong presence of local electromagnetic forces, we insert the Newton-Lorentz force equation, which describes the behavior of forces due to the presence of electric and magnetic fields:

$$\frac{\partial f}{\partial t} + \vec{\boldsymbol{u}} \cdot \frac{\partial f}{\partial \vec{\boldsymbol{r}}} + \frac{q}{m}\left[\vec{\boldsymbol{E}} + \vec{\boldsymbol{v}} \times \vec{\boldsymbol{B}}\right]\frac{\partial f}{\partial \vec{\boldsymbol{u}}} = S_{coll} \tag{2.15}$$

This is the traditional Boltzmann equation describing the phase space of a plasma. To determine a time-averaged quantity ϕ of the plasma, we multiply the Boltzmann equation by ϕ, and integrate over the velocity space. This allows us to take moments of the Boltzmann equation for quantities, but this mathematically will always introduce the next-higher moment in the calculated moment, leading to an infinite number of moments and no mathematical closure to the system. In order to close this process, we introduce constitutive relations regarding the heat flow (usually adiabatic or isentropic relations are used [19,20]). For brevity, the derivation of these moments will not be repeated here; they can be found in standard literature [19–21], and result in the typical Navier-Stokes compressible, viscous equations, which for the summed totals species is: [20]

$$\frac{Dn}{Dt} + n\nabla \cdot \vec{\boldsymbol{u}} = \frac{\partial n}{\partial t} + \vec{\boldsymbol{u}} \cdot \nabla n + n\nabla \cdot \vec{\boldsymbol{u}} = 0 \tag{2.16}$$

$$\rho\frac{D\vec{\boldsymbol{u}}}{Dt} + \nabla \cdot \bar{\bar{\boldsymbol{\tau}}} + \nabla p = \rho_e(\vec{\boldsymbol{E}} + \vec{\boldsymbol{u}} \times \vec{\boldsymbol{B}}) + \vec{\boldsymbol{j}} \times \vec{\boldsymbol{B}} \tag{2.17}$$

$$\rho\frac{DH}{Dt} - \frac{\partial p}{\partial t} = -\nabla \cdot \vec{\boldsymbol{q}} - \nabla \cdot (\vec{\boldsymbol{u}} \cdot \bar{\bar{\boldsymbol{\tau}}}) + \vec{\boldsymbol{E}} \cdot \vec{\boldsymbol{J}} \tag{2.18}$$

Here $\bar{\bar{\boldsymbol{\tau}}}$ represents the fluid shearing stress tensor and p the hydrostatic pressure, which together comprise the full pressure tensor, and $\vec{\boldsymbol{j}}$ is the current density field.

An appropriate model must be introduced for the shearing stress tensor $\bar{\bar{\boldsymbol{\tau}}}$ and electrical conduction current density $\vec{\boldsymbol{j}}$. A variety of models may be applied, but of course they must properly model the fluid to be examined. The typical approach is to apply the Newtonian assumption from a Couette flow to model the relation between the stress tensor and the strain for the fluid, and to assume the validity of the generalized Ohm's law. This makes the assertion that the stress induced in the fluid is directly proportional by some coefficient of viscosity to the strain endured in the fluid. For most fluids and plasmas, this approximation gives a good match between theory and experiment. For certain other fluids, higher-order terms must be added to the Newtonian assumption. In our case, the Newtonian assumption will suffice. The stress tensor that results from the Newtonian assumption is:

$$\bar{\bar{\boldsymbol{\tau}}}_{ij} = -\eta\left(\frac{\partial u_i}{\partial x_j} + \frac{\partial u_j}{\partial u_i}\right) + \frac{2}{3}\eta\delta_{ij}\nabla \cdot \vec{\boldsymbol{u}} \tag{2.19}$$

The electrical conduction current density $\vec{\boldsymbol{j}}$ may be related to the electric and magnetic fields $\vec{\boldsymbol{E}}$ and $\vec{\boldsymbol{B}}$ by use of the generalized Ohm's law, given as:

$$\vec{\boldsymbol{j}} = \sigma\left(\vec{\boldsymbol{E}} + \vec{\boldsymbol{v}} \times \vec{\boldsymbol{B}} - \beta(\vec{\boldsymbol{j}} \times \vec{\boldsymbol{B}})\right) \tag{2.20}$$

The first two terms are the conduction current of the fluid. The last term is introduced by the Hall current, induced by the Hall effect. The β coefficient is the Hall parameter, which dictates the influence the Hall effect exerts on the overall current. Two important currents have already been removed from the above relation: the convective current introduced by charge transport, and the ion slip current. Convection current does not play a present role in plasma behavior due to the overall charge neutrality of the fluid, and ion slip does not contribute significantly for fluids that are modeled well by continuum assumptions. Since the plasma we will be dealing with is largely continuum and is considered overall charge-neutral, we do not consider these currents to play a prominent role in the behavior of the plasma.

Another important consideration is if turbulence appears in the fluid. If it does, the equations may be rewritten above to include a Reynolds stress tensor term and determine the mean and average deviation terms; however, due to the typical viscosities of the materials [22], small length scale, and taking the largest velocity encountered during simulation, all flow appears to be laminar with very small Reynolds numbers. The MACH2 code is capable of modeling turbulent flow as well, in the case that it does appear.

Appropriate boundary and initial conditions must be applied as well, in order that a unique solution exist. As just mentioned, the plasma is largely observed as a continuum fluid, and hence the typical fluid boundary conditions may be used; the size and density of the plasma justify the use of the continuum assumption, and velocity slips are usually neglected. The no-slip boundary condition applies to interfaces between the plasma and solid, and the no-shear boundary condition applies to vapor-vapor interfaces. Although it might initially be questioned if micrometer-length scales contain enough particles to be considered a continuum, this plasma is a typical laboratory-density plasma, which indicates that the number density within a micrometer cube of volume is still considerably high.

In addition to the fluid equations of motion, electrodynamic processes are also important, and Maxwell's electrodynamic equations must be accounted for as well. In their canonical form, these are eight linear first-order partial differential equations, given as [23]:

$$\nabla \cdot \vec{\boldsymbol{E}} = {\epsilon_0}^{-1} \rho_e \tag{2.21}$$

$$\nabla \cdot \vec{\boldsymbol{B}} = 0 \tag{2.22}$$

$$\nabla \times \vec{\boldsymbol{E}} = -\frac{\partial \vec{\boldsymbol{B}}}{\partial t} \tag{2.23}$$

$$\nabla \times \vec{\boldsymbol{B}} = \mu_0 \vec{\boldsymbol{j}} + \mu_0 \epsilon_0 \frac{\partial \vec{\boldsymbol{E}}}{\partial t} \tag{2.24}$$

It is well-known in electrodynamics that a particle undergoing an acceleration radiates or absorbs light energy [23]. A free electron that undergoes no change in motion cannot radiate or absorb photon energy, lest conservation of energy and momentum are broken. Therefore, free electrons only radiate or absorb photons when a collision occurs in the plasma. It is then natural to expect the transfer of energy from the laser light to the plasma electrons to depend strongly on collision frequency. The process of emission and absorption of photon energy by electrons is formally known as *bremsstrahlung* and *inverse bremsstrahlung*, respectively. A highly collisional plasma will see an abundance of emission and absorption processes, which result in a very complex energy transfer mechanism of photon energy to the plasma. In the case of incident laser light striking a plasma, inverse *bremsstrahlung* processes must dominate in order that a net absorption of photon energy occurs. Of course, as mentioned this process is inherently dependent on the collision frequency of the plasma.

Previous investigations [24] have been made on the use of continuous-wave and repetitively-pulsed lasers for initiating ablation of solid propellants. The continuous-wave laser operation heats the vapor formed by ablation via inverse *bremsstrahlung* processes, but these processes are inherently unstable. Laser-heated flows initiated by continuous-wave operation are very complex and not well understood [24]. However, repetitively-pulsed lasers may produce ideal propulsion plasmas if the laser pulse duration is short enough [24]. Initial investigations of pulsed laser propulsion provided only a few percent efficiency, but this was because the pulse duration was too long [24]. If the pulse duration is short, the mechanism by which thrust is achieved is via a continuously weakening shock wave that is initiated by the laser and propagates through the propellant, transferring laser energy to kinetic energy of the propellants.

2.3 MACH2: A 2D Magnetohydrodynamic Code

The equations governing the laser-plasma interaction mediated by the ablation of a solid or liquid propellant into a plasma are clearly very difficult; they involve the solution of the fluid dynamic equations, which are five predominantly second-order and highly nonlinear partial differential equations, with necessary constitutive models introduced for the stress and current density, which closes the system mathematically. Furthermore additional necessary boundary and initial conditions are introduced to satisfy the determination of a unique solution. The electrodynamic equations (Maxwell's equations) also play an important role in the determination of the radiation interaction with matter; these consist of eight linear first-order partial differential equations which are typically much easier to solve. However, the overall problem, as well as any additional considerations (heat transfer effects, for example) quickly make an analytical solution insurmountable without numerous simplifying assumptions, most of which would tend to eliminate the interesting physics anyway. Therefore, a numerical solution is sought as an iterative form of these equations.

For the purposes of the investigations made in this thesis, it is sufficient to use a two-dimensional magnetohydrodynamic code, called the Multiblock Arbitrary Coordinate Hydromagnetics code, or Mach2. A much more comprehensive overview of the Mach2 code than presented here can be found in the review provided by Robert E. Peterkin, Michael H. Frese and Carl R. Sovinec [25], the available technical reports regarding the usage of the code by Michael H. Frese and John J. Watrous [26], or the published literature on the algorithms implemented in the code [25, 27–29]. Only a brief overview of the available and published equations and procedures employed by Mach2 is given here.

Mach2 is a two-dimensional magnetohydrodynamic single-fluid code designed for the study of unsteady, collisional plasma behavior [25]. It is an arbitrary Lagrangian/Eulerian code, wherein Faraday's law is iterated by a Lagrangian advance followed by a remap of the magnetic field from the Lagrangian frame to the computational grid. [25, 27] The computational grid itself may be Eulerian (in the frame of the laboratory), Lagrangian (in the rest frame of the fluid flow), or in some arbitrary state between. [25] For the purposes of investigation presented here, our simulations were solved in the Eulerian frame of the spacecraft.

The code relies on a quadrilateral two-dimensional grid geometry that is user-specified, aligned corner to corner, and calculations are performed in either a two-dimensional cartesian frame or a cylindrical axisymmetric frame, as specified by the user. The quadrilaterals define the geometry of the hexahedral cells that are used for the computation. [25] All components of three-dimensional vectors are retained during the computation; however, no quantity is allowed to vary with the direction normal to the computational plane. [25] The magnetohydrodynamic equations are solved in an iterative fashion by considering finite-volume integrations of flux through the surfaces of adjoining hexahedral cells; the iterations rely on book-keeping of conservation quantities, and MACH2 raises error exceptions to execution when nonconservation is achieved. [25]

MACH2 solves the magnetohydrodynamic equations iteratively over a specified time range for a given geometry with specified initial and boundary conditions. The magnetohydrodynamic equations may be approached in a variety of manners (resistive, turbulent, two-fluid, etc.); in our investigations, the ideal magnetohydrodynamic equations were used, when applicable, with no magnetic dissipation present. The fluid dynamic equations retain their viscous and compressible form, introducing the typical Navier-Stokes equations representing the conservation of mass, momentum and energy. The electrodynamic equations introduce Faraday's law, Ampere's law with neglected displacement current, Gauss' law and the constraint of no magnetic charge to describe the conduction of current in the fluid.

For a charge-neutral magnetic fluid of mass density ρ, velocity $\vec{\boldsymbol{u}}$, and with a present magnetic field $\vec{\boldsymbol{B}}$, the ideal magnetohydrodynamic equations consist of the fluid dynamic equations (with split energy equations for ions and electrons), and Faraday's law, all given as: [25]

$$\frac{\partial \rho}{\partial t} + \nabla \cdot (\rho \vec{\boldsymbol{u}}) = 0 \tag{2.25}$$

$$\rho \frac{\partial \vec{\boldsymbol{u}}}{\partial t} + \rho \vec{\boldsymbol{u}} \cdot \nabla \vec{\boldsymbol{u}} = \nabla \cdot (-\gamma^{\alpha\beta}(P_e + P_i + Q) + M^{\alpha\beta}) \tag{2.26}$$

$$\rho \frac{\partial E_i}{\partial t} + \rho \vec{\boldsymbol{u}} \cdot \nabla E_i = -P_i \nabla \cdot \vec{\boldsymbol{u}} + \Phi_{ei} \tag{2.27}$$

$$\rho\frac{\partial E_e}{\partial t} + \rho\vec{\boldsymbol{u}}\cdot\nabla E_e = -P_e\nabla\cdot\vec{\boldsymbol{u}} + \vec{\boldsymbol{J}}\cdot\vec{\boldsymbol{E}} - \Phi_{ei} \tag{2.28}$$

$$\nabla\times\vec{\boldsymbol{E}} = -\frac{\partial\vec{\boldsymbol{B}}}{\partial t} \tag{2.29}$$

where $\gamma^{\alpha\beta}$ is the spatial metric tensor in contravariant components (which corresponds to the unit dyad in orthogonal coordinate systems) and $M^{\alpha\beta}$ is the Maxwell stress tensor, given as

$$M^{\alpha\beta} = \frac{1}{\mu_0}\left(B^\alpha B^\beta - \frac{1}{2}B^2\gamma^{\alpha\beta}\right) \tag{2.30}$$

Q is a term introduced for numerical stability reasons [25] and Φ_{ei} is an electron-ion coupling term. [25] The generalized Ohm's law may be introduced to determine the relation of the electric field $\vec{\boldsymbol{E}}$ and the magnetic field $\vec{\boldsymbol{B}}$.

The electrodynamic equations are still strongly coupled, which creates difficulty for a numerical solution. However, by examining a scale analysis of the electrodynamic equations of Maxwell, it can be shown [20, 30] that the displacement current scales as the ratio of the velocity scale to the speed of light. For most cases, this indicates that the displacement current is negligible; only near relativistic speed scales will the displacement current contribute significantly. By virtue of similar scale analyses [30], the convective current flow (current flow due to charge transport) can also be neglected, as may the force due to the electric field. The collective assumption of dropping these terms from the equations is called the *magnetohydrodynamic* assumption, for which the equations are named. Following this assumption, the current density can now be determined by Ampere's law,

$$\vec{\boldsymbol{j}} = \frac{1}{\mu_0}\nabla\times\vec{\boldsymbol{B}} \tag{2.31}$$

Furthermore, the numerical solution of these equations should preserve the magnetic monopole constraint,

$$\nabla\cdot\vec{\boldsymbol{B}} = 0 \tag{2.32}$$

Finally, mathematical closure of these equations is achieved by introducing thermodynamic relations of state for electrons and ions. MACH2 allows the equation of state to be specified per material, which may consist of experimental tabular data for different materials (provided by the Sesame tables), perfect gas approximations, Van der Waals approximations or the Mie-Gruneisen equation of state. [2, 28] As discussed earlier, the propellant we wish to explore is polyvinylchloride polymer (PVC), as well as exploring the differences in using other propellants as well (to be discussed in Chapter 4). It is non-sensical to model the equations of state for these propellants as gas or liquid, since they are polymer and retain several solid properties. Therefore, it is necessary to use tabular equation-of-state data to model these propellants. However, equation-of-state information for PVC is not readily available for use in Mach2. Therefore, in the research investigations made here, we model the propellant as polytetrafluoroethylene (Teflon®), for which tabular equation-of-state data is abundant (this is discussed more in the modeling section of Chapter 4).

The perfect gas law is simply given as

$$p = nk_BT \tag{2.33}$$

While this may be adequate for gases and plasmas, it is inappropriate to model a solid. To this end, the Mie-Gruneisen equation of state can be specifically used for modeling solids, particularly when shock compressions are introduced. A variety of forms of the Mie-Gruneisen equation exist; the given form used by the Mach2 solver is [29]:

$$\begin{aligned} p = \frac{\rho T(1-n_f)}{fA} + \frac{\rho c_{s0}^2(1-\frac{\rho_0}{\rho})}{1-\frac{1}{2}(\gamma_0+1)(1-\frac{\rho_0}{\rho})} \cdot \\ \cdot \left[\frac{1}{2}(\gamma_1-1)(1-\frac{\rho_0}{\rho}+\frac{\rho_0}{\rho}\cdot\left(1-\frac{1}{2}(\gamma_0-1)(1-\frac{\rho_0}{\rho}\right)\right] \end{aligned} \tag{2.34}$$

The equations of state modeled in the investigations made here regard the gases and plasmas as adequately described by the perfect gas law, while solids with known Sesame tables employed tabular equation-of-state data; those solids that did not have any known tabular data were modeled with the Mie-Gruneisen equation.

The detonation module accompanying the Mach2 code simulates the introduction of an explosion in a material present during simulation. Available literature concerning the detonation modeling capabilities is given by Michael H. Frese and John J. Watrous [28,29].

The investigations made here make use of the detonation module for the energetic propellant simulations described in Chapter 4. The MACH2 code requires two specific conditions be met for a detonation to occur: *(i)* that the specific internal energy in any cell surpass a known threshold specific internal energy pertaining to the material being modeled, and *(ii)* that numerical constraints be introduced to avoid nonphysical conditions [29]. The input file allows specification of the threshold energy and energy released upon detonation. In addition, the precedent set in the literature [28] tends to specify the undetonated explosive material as described by a Mie-Gruneisen equation of state; the parameters for the equation of state must match that of the material being modeled. The specific details of the material models used in these simulations is the content of Chapter 4, and the appropriate propellant modeling will be more fully explored there.

The MACH2 code is used in these investigations to simulate the physics of laser-plasma interactions. The code allows for a variety of laser setups [2, 25]; in our investigations, the laser was simulated as closely as allowed by the code to the announced setup for the commercial microthruster design (see design details in [1, 8, 16]). To this end, the laser module of MACH2 was also used extensively in these investigations. The code simulates the addition of energy via a focused laser that supports a nonequilibrium radiation diffusion model, since the effect of radiative losses would incur energy budgeting errors [31]. The laser module deposits appropriate energy due to laser absorption, simulating inverse *bremsstrahlung* laser absorption processes, and the criterion for the initiation of laser-supported detonation by the laser module is dependent on the space-dependent and time-dependent electron number density, which determines the surface at which the detonation will be initiated [31]. This laser absorption model was used in the MACH2 code to simulate the laser ablation of the propellants, both in previous work [2] and in these investigations. The process was set to predominantly depend on inverse *bremsstrahlung* processes alone.

It is important that the simulations report the data being accumulated in a fashion that allows for postprocessing and later analysis. The MACH2 code accomodates this need by providing methods of writing history data from the simulation; the history output desired is specified by the user, and the code records all instructed values to exported files for later evaluation. This method of collecting data is used extensively in this work. Most of the performance evaluation of each proposed case was quantified and compared after the simulation execution. To this end, additional code was written for postprocessing and analysis, which performed necessary time integrations of desired quantities, cumulative sums and other needed values. The data received from the simulations and the methodology of postprocessing will be described in Chapter 3, where the postprocessor and calculations are explained.

Chapter 3

Methodology

3.1 Previous Computational Simulations of Microthruster Operation

The previous computational work [2] succeeded at demonstrating a computational model of the microthruster operation with a solid propellant. The simulation was executed for various laser energies between 20μJ and 2mJ to qualitatively demonstrate the operation of the microthruster. The geometry of the computational domain used in previous simulations [2] is shown in Figure 3.1; this is a two-dimensional axisymmetric slice of the microthruster, with blocks enumerated by different colors. Figure 3.2 shows a pseudocolor two-dimensional contour plot of the density within the computational domain for the 20μJ case, re-executed in Mach2 with the new methodology described in this chapter; Figure 3.3 shows similar results for the 2mJ case. The higher-density regions correspond to the solid propellant, while the lower-density regions correspond to the plasma plume and background gas. The results of these test cases are shown in Table 3.1. Since the work of this thesis aims to expand this simulation for other microthruster operation modes, we examine the geometry and methodology of this simulation in some detail here.

Figure 3.1 presents the consistent geometry used in the previous simulations [2]. Blocks 1 and 2 comprise the optically-transparent substrate present in the microthruster design [2, 3, 8]. In previous experimental work [3], substrates composed of cellulose acetate, PET and Kapton^{TM} polyimide resin were tested; the polyimide resin seemed to work optimally for most setups. This substrate was simulated with the same properties as the Teflon® propellant modeled here, but does not absorb any of the laser radiation. The laser is set to propagate from the lower boundary of Block 1 and given a Gaussian spatial variance profile. The laser energy was retested for 20μJ and 2mJ of total pulse energy, radiated in a Gaussian form with a 0.5μs FWHM pulse duration, with the peak laser energy occurring at 0.75μs. Blocks 3, 4, 5 and 6 are composed of the Teflon® propellant, using SESAME tabular data for the equation of state and with default densities of 2152$\frac{kg}{m^3}$. Blocks 3 and 4 are separated from Blocks 5 and 6 due to previous attempts to change the laser absorption parameters at the focal point of the laser. Blocks 7 and 8 model the external space of the microthruster; this region is set to dry air at a pressure of 5mtorr, modeled as a perfect gas to simulate the experimental conditions of previous experiments [14].

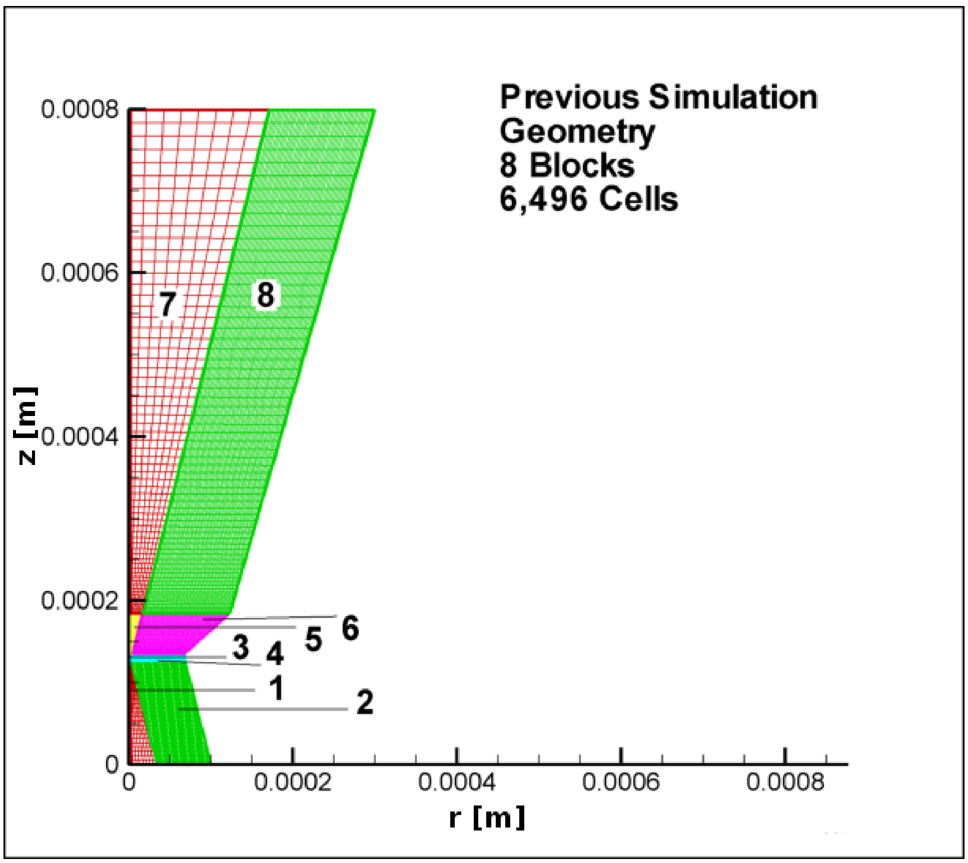

Figure 3.1: Geometry used in previous simulations [2] with the MACH2 code for micro-thruster operation.

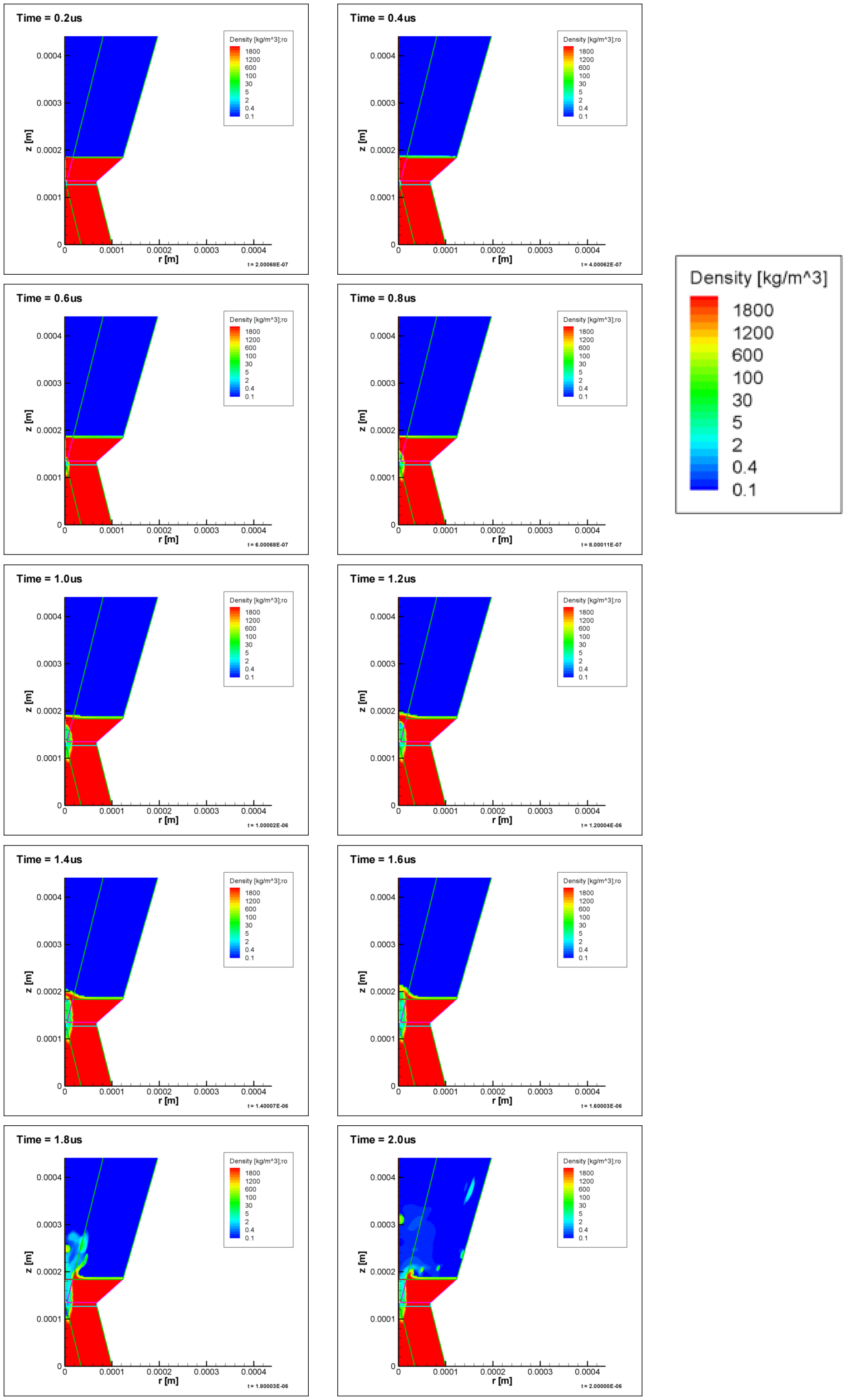

Figure 3.2: The 20μJ baseline test case with passive solid propellant. These results were obtained from re-execution, and match the results presented in [2]. Time shown from 0.2 to 2.0 microseconds.

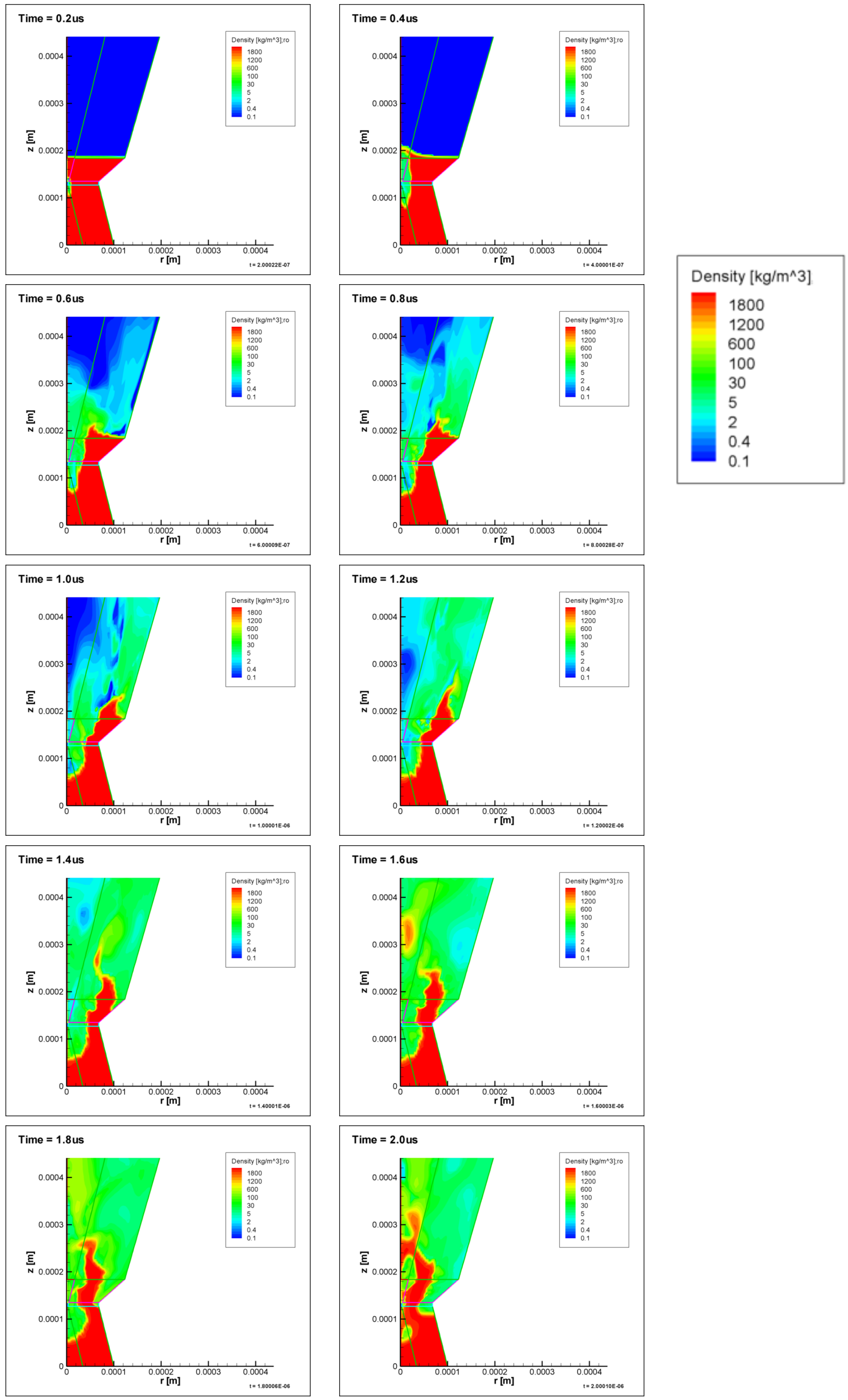

Figure 3.3: The 2mJ baseline test case with passive solid propellant. These results were obtained from re-execution, and match the results presented in [2]. Time shown from 0.1 to 1.0 microseconds.

The results of this simulation are shown in Table 3.1. The 20μJ and 2mJ cases have been performed again in MACH2 for the purposes of this thesis with the history source rewritten for the MACH2 code. This allowed a more transparent collection of the data simulated. These results compare very well with the published figures [2], except for the specific impulse, which is off by an order of magnitude from previous simulation. This difference occurs because of the wide difference in exhaust velocity calculable by different measures. The exhaust velocity measures made in this thesis are considered closer in method to that performed in experimentation. This simulation, as well as a calibration of the 2mJ case for a nozzle, was used as a baseline test for comparison with the other modes of operation explored in this thesis.

Due to the nature of the MACH2 code for simulating these characteristic plasmas, only microsecond-regime calculations were available [2]. Therefore, the laser pulse duration was much shorter than in most of the prototypes built [3,8]. Typically, millisecond-length pulses are used in the prototypes [1,16]. The use of microsecond pulses introduces a much higher wattage, and hence we can expect to see quantitative differences between the simulations and experiments. Indeed, as shown in Table 3.1, the coupling coefficients are an order of magnitude higher than typical experimental coefficients of the same material. The thrust is also an order of magnitude higher. The specific impulse in these calculations totally disagrees with previous simulation calculations [2], because the velocity is highly variant and a different measurement of the velocity was used than previously (this velocity tends to be closer to the experimental value, but follows naturally from the measurements made in the history).

3.2 Proposed Methodology and History Postprocessing

Starting from the previous computational work presented [2], modifications were made in a step-wise fashion to the simulation in order to accomplish the development of a new computational model of operation, as per each of the enumerated cases in Chapter 1. The initial geometry was modified and the laser parameters changed until a stable simulation was found to execute long enough that laser ablation had finished (although typically plasma plume expansion had not; this did not significantly affect the measurements made

Table 3.1: Results for the previous baseline simulations [2], calculated using the new Mach2 history and postprocessors.

	Baseline Tests	
Parameter	2mJ	20μJ
Mass Ejected, [ng]	1.37	0.137
Avg. Laser Power, [W]	1000	200
Avg. Thrust, [mN]	830	64
Impulse Bit, [μNs]	3.33	1.62
Avg. Exhaust Velocity, [m/s]	2,439	1,185
Coupling Coefficient C_m, [N/MW]	1,664	8,119
Specific Impulse I_{sp}, [s]	250	120
Ablation Efficiency, η_{ab}, [%]	9.1	26.4

during the simulation, but did significantly alter the approach of measurement taken, as discussed below).

The history source of Mach2 was rewritten for different simulations in order to gather values needed for analysis and comparison. The accuracy of the history was verified by rerunning the previous simulations with the new history, and the published performance parameters were confirmed (except for specific impulse, as explained in the previous section). Two data postprocessors were written outside of the Mach2 code, the first in Python and the second in MatLab. The separation of postprocessing between two codes occurs merely for the convenience of the programmer. The Python postprocessor was responsible for determining the mass ejected from the propellant fuel tape, desegmenting the output history data for further processing and dotting the nozzle pressure data with the thruster axis (determining the azimuthal component, which is of interest). A calibration of the Python program to verify its accuracy was performed, as discussed below. The MatLab program then assumed the remainder of the analysis, by determining the instantaneous thrust, impulse bit, velocity, coupling coefficient, specific impulse and ablation efficiency. The history recorded the total kinetic energy and total momentum along the thruster axis every time Mach2 called the history routine, which were used for determining check values. A consideration of the details of calculation for the different parameters determined follows.

3.3 Mass Measurements

In previous work, often mass passing a certain line within the computational domain has been totaled, and if this line is placed properly and the simulation executed for long enough, this technique will allow for adequate collection of the mass ejected from a thruster. This technique was not considered adequate for these simulations, since a simulation time long enough for all of the plasma to leave the system would be extraordinarily wasteful of computational resources and time, and because significant amounts of mass exited the computational domain along the sides rather than along the axis. Instead, a Python program was written to integrate the mass at or above the solid density in a given region of the thruster. This technique could then be applied to the initial condition of the thruster and to the final condition of the thruster, and the difference is taken as the mass ejected. This is similar in practice to techniques used experimentally in the literature, wherein the crater diameter of the ablation site is measured with SEM visualization, and the amount of mass calculated as an oblique cylinder removed [8]. A calibration of this Python program was executed wherein the entire mass in the computational domain was integrated for initial conditions; the result was compared to the MACH2 bookkeeping, and the difference was less than 1% error.

A further confirmation of the mass ejected was made by recording the total kinetic energy $E_k = \frac{1}{2}\Delta m v_{ex}^2$ and total momentum along the thruster axis $p_y = \Delta m v_{ex}$. These values were recorded per history write, so if there were I history writes total, then there is a measured array of total kinetic energy and total momentum along the thruster axis, ${E_k}^i$ and ${p_y}^i$, where $i \in \{1, ..., I\}$. Since the simulation is in the reference frame of the spacecraft, the only significant motion in the computational domain must belong to the plasma plume. In such a case, this constitutes a system of $2I$ equations with $2I$ unknowns, the mass and average velocity of the plasma plume at each history write. For each time interval i, this can be solved to determine the mass and average velocity along the thruster axis Δm^i and ${v_y}^i$ for $i \in \{1, ..., I\}$. Ideally, the mass of the plasma plume could be determined by this method simply by looking at the last value of the mass recorded, Δm^I, but since mass leaves the computational domain, this value would only give the mass of the plume still within the computational domain. To avoid this, the difference in mass between every two timesteps can be calculated, which results in an array Δm^j, where $j \in \{1, ..., I-1\}$; likewise for the velocity. These arrays, Δm^j and ${v_y}^j$, represent the contribution of mass and velocity made every history write. Furthermore, data was collected of any material passing across the boundaries of the computational domain along the axis of the thruster; therefore, we have further separate arrays of Δm_e^j and ${v_e}^k$ as well, where $k \in \{1, ..., I\}$, and these represent the mass ejected across the computational boundary dotted in the direction of the thruster. If we consider them constant along the intervals between history writes, we can total the mass contributions to determine the full amount of mass in the plasma plume,

$$\Delta m^{(check)} = \sum_{i=1}^{I-1} \Delta m^j = \sum_{i=1}^{I-1} (\Delta m^{(i+1)} - \Delta m^i) + (\Delta m_e^{i+1} - \Delta m_e^i) \tag{3.1}$$

Notice that if there is no mass ejected across the computational domain, $\Delta m_e = 0$, and hence we reduce this to a telescoping series, which gives us exactly what is expected – simply the difference in the first and last mass measurements of the plume.

A similar technique may be applied as well for a momentum calculation,

$$\Delta p^{(check)} = \sum_{i=1}^{I-1} (\Delta m^j {v_y}^j) = \sum_{i=1}^{I-1} \left[(\Delta m^{(i+1)} + \Delta m_e^{(i+1)}) {v_y}^{(i+1)} - (\Delta m^i + \Delta m_e^i) {v_y}^i \right] \tag{3.2}$$

These checks were used simply to confirm the order of magnitude of the simulations executed. They agreed on the order of magnitude of the Python mass ejected, but were occasionally off by an order of magnitude from the average velocity. This occurred because the average velocity varied much more widely than the mass ejected. The checks generally estimated a mass about 50% of that calculated by the Python program and a velocity about two to ten times the magnitude of the average velocity calculated by postprocessors. Because of comparisons to the MACH2 bookkeeping, the Python mass ejected and average velocity calculated in Section 3.6 are considered more accurate and used as the primary measurements.

3.4 Thrust Measurements

The rocket equation given in Chapter 2 could be used to approximate the thrust experienced during the simulation, but unfortunately a measurement of $\dot{m}$ is very difficult to make. Therefore, an alternate approach was taken wherein the thrust is considered equal by reaction to the product of pressure and area applied to the walls of the computational domain. In the cases of the previous work [2] and the energetic propellant geometries, the product of the pressure on the base of the thruster geometry and the corresponding area can be equated to the thrust, since no other forces are acting on the system. In the case of the axisymmetric nozzle, this calculation is a little more difficult due to the presence of several walls at arbitrary angles. The product of pressure and area of each wall was taken, dotted with the thruster axis and taken in the opposite sense, and summed to determine the thrust applied,

$$T_y{}^i = \sum_{k=1}^{\text{Walls}} \left[\left(\left(A_k \vec{\boldsymbol{n}}_k \right) \cdot \vec{\boldsymbol{y}} \right) \right]^i \tag{3.3}$$

Here i is an index referring to the integer multiple of the time between calling the history routine, and k indicates the wall of the computational domain; $\vec{\boldsymbol{n}}_k$ indicates the normal vector of the wall surface, $\vec{\boldsymbol{y}}$ refers to the thruster axis (the azimuthal direction, in the simulations presented in this thesis), and A_k refers to the force acting on the wall k (the product of pressure and area of the wall, as calculated by MACH2.) The average thrust is used to evaluate the thrust performance of the microthruster operation mode,

$$T_{y-avg} = \text{average}(T_y{}^i) = \frac{1}{I} \left\{ \sum_{i=1}^{I} \sum_{k=1}^{\text{Walls}} \left[\left(\left(A_k \vec{\boldsymbol{n}}_k \right) \cdot \vec{\boldsymbol{y}} \right) \right]^i \right\} \tag{3.4}$$

This method was implemented in the postprocessing and is taken as the thrust force resulting from the micro-thruster operation.

3.5 Impulse Bit Measurements

Once the thrust has been determined, the impulse bit may be calculated by time-integrating the effective total thrust,

$$p_y = \int_0^t T dt \tag{3.5}$$

For the effective thrust array calculated above, we can discretize the integration to use the history-written thrust. Here the average of the thrust between two time intervals is used as the effective thrust between history writes, and the difference between the times recorded for the history writes is used as the time differential,

$$p_y \approx \sum_{j=1}^{I-1} \text{average}({T_y}^j) \Delta t^j \approx \sum_{i=1}^{I-1} \frac{1}{2} \left({T_y}^{(i+1)} - {T_y}^i \right) \left(t^{(i+1)} - t^i \right) \tag{3.6}$$

This value can be compared to the above calculation of the impulse bit from the system of known E_k and p_y for a check on this computation. The momentum check, as described in more detail in Section 3.3, tended to be on the same order of magnitude as the value calculated from the history-postprocessed equation above. The equation given above was used for making the determination of impulse bit, and is used in the presentations given in the results.

3.6 Exhaust Velocity Measurements

The exhaust velocity varied with a much wider error than most measurements, sometimes being up to an order of magnitude different from expected by the existing experimental data. This is because giving a specific velocity to the entire plasma plume is very difficult without making gross assumptions regarding the plasma movement and characteristics. The velocity was taken as the quotient of the impulse bit calculated and the mass ejected as determined by the Python program,

$$v_{ex} \approx \frac{\Delta p}{\Delta m} \tag{3.7}$$

This effectively mass-averaged velocity tended to be lower than the expected characteristic velocity of the propellant, but this calculation was used as a conservative estimate of the velocity for the determination of specific impulse and ablation efficiency.

3.7 Laser Momentum Coupling Coefficient Calculations

The laser momentum coupling coefficient was defined in Chapter 2 as the ratio of the impulse provided to the incident laser energy. This is effectively synonomous to the ratio of thrust produced to incident laser power on the propellant target. The impulse bit of the plume was calculated as per the description in Section 3.5. The incident laser energy was already known from the energy set before the start of the simulation; therefore, the coupling coefficient could be calculated easily,

$$C_m = \frac{\int F dt}{W} \approx \frac{1}{W} \sum_{i=1}^{I} \left({T_y}^{(i+1)} - {T_y}^{i} \right) \left(t^{(i+1)} - t^{i} \right) \tag{3.8}$$

The coupling coefficient is an important parameter for comparisons between simulation and experiment because it is so readily determined in experimentation. It is perhaps the most easily determined factor for an experimental setup. The above determination will be used in the postprocessing for calculating the coupling coefficient.

3.8 Ablation Efficiency

The ablation efficiency is defined as the ratio of the kinetic energy to the incident laser energy, rendering the quantity dimensionless. The Python ejected mass was used as the effective mass and the average velocity determined as the division of Δp and Δm to determine the kinetic energy. The laser incident energy is known from the simulation setup. Therefore, the ablation efficiency may be easily determined,

$$\eta_{ab} \approx \frac{\frac{1}{2}\Delta m v_{ex}^2}{W} \approx \frac{1}{2W} \left(\frac{\Delta p^2}{\Delta m} \right) \tag{3.9}$$

It should be remembered that ablation efficiencies for passive targets must be less than unity but may be greater than unity for exothermic materials. This is due to the extra chemical release provided by the exothermic reaction. The ablation efficiency also often accounts for large discrepancies between configurations with very different results; significantly different efficiencies indicate higher or lower available specific impulses and coupling coefficients for missions.

Chapter 4

Energetic Propellants

4.1 Introduction to Energetic Propellants

Early designs for the subkilogram microthruster used a solid form of propellant, namely, polyvinylchloride (PVC) polymer, as an ablation fuel [3, 22]. Polymers were considered ideal candidates due to their low thermal conductivity; the laser pulse length and ablation threshold demand low heat transfer effects if ablation is to occur. Solid forms of propellant are ideal in that they do not require extra storage equipment and do not exhibit abnormal fluid behavior during ablation.

However, later considerations (beginning around 2004) of the propellant realized that much greater efficiency could be achieved by the use of an *energetic* or *exothermic* propellant. These terms are synonymous to indicate that the propellant has an active chemical arrangement that may be broken to release energy during ablation. Therefore, the ablation of the energetic propellant releases extra chemical energy, which increases the kinetic energy of the propellant exiting the thruster; this requires less energy from the laser to achieve the same thrust.

With the attractive realization of the energetic addition of energy, extensive investigations were made in experimental demonstrations of different energetic propellants for use in the microthruster design. Available comparisons from several experiments [1, 8, 12–15] are presented in Table 4.1. It is clear from these values that significant increases in performance can be realized by the use of energetic propellants. Commonly explored propellants

Table 4.1: Collective previous experimental measurements of performance parameters for energetic materials.
[1] Indicates percent by mass carbon nanopearl doping, [2] indicates per cent by mass IR dye Epolin 2057 doping, [3] indicates experiment was executed at optimal ablation efficiency, — indicates values were not reported.

A compilation of previous experimental measurements of performance parameters							
Propellant	I, GW/cm^2	τ, ms	C_m, N/MW	I_{sp}, s	Thrust, μN	v_{ex}, ms^{-1}	η_{ab}, %
PVN+10%C[1] [13]	403	1	310	137	113	2500	21
PVN+10% ink [13]	403	1	256	155	94	2500	19
PVN+1%IR[2] [13]	175	1	103	76	35	2500	4
GAP+C [13]	175	1	1960	188	392	2500	181
GAP+5% ink [13]	150	1	1970	190	394	2500	183
GAP+1%IR [13]	230	1	1574	256	167	2500	198
PVC+5% ink [13]	570	2.5	94	189	137	2500	8.7
NC+2%C [13]	400	1	471	183	179	2500	42
PVC+C[3] [14]	7-23J/cm^2	—	120	650	—	—	—
PVN+C[3] [14]	7-23J/cm^2	—	850	2320	—	—	—
GAP+C[3] [14]	7-23J/cm^2	—	1170	500	—	—	—
GAP+IR[3] [14]	7-23J/cm^2	—	2000	240	—	—	—
PVC+5%C [1]	5W	1.5	60	750	10mN	—	20
GLYN+2%C [1]	5W	1.5	1280	116	10mN	—	73
GAP+IR [1]	5W	1.5	1300	200	10mN	—	125
GAP+1%C [1]	5W	1.5	3000	160	10mN	—	235
PVN+5%C [1]	5W	1.5	116	2890	10mN	—	164
GAP+C [15]	25J/cm^2	6	865	867	—	8502	368
GAP+IR [15]	25J/cm^2	6	1574	256	—	2510	198
PVN+C [15]	25J/cm^2	6	310	137	—	1343	21
PVC+C [15]	25J/cm^2	6	635	159	—	1559	49

included glycidyl azide polymer (GAP), polyvinylnitrate (PVN), nitrocellulose (NC) and polyglycidylnitrate (GLYN).

The use of energetic liquid polymers necessarily involves new fluid phenomena occurring in the ablation process, which may be problematic in the microthruster design. It has been demonstrated [22] that the use of liquid polymers introduces new fluence-dependent and viscosity-dependent effects (splashing, spallation, etc.) that may destroy the improved efficiency altogether. Experimental research has shown that high-viscosity liquid polymers tend to minimize these effects such that performance improvements may still be practically seen [22]. The splashing and other fluid phenomena does not occur until the hundreds of microseconds time scale [14, 22], so the simulations presented here preclude any study of anomalous fluid phenomena due to the shortened time scale. Since the polymers modeled here have high viscosity, the fluid effects are considered minimized due to previous research [22].

Since the replacement of a passive solid target with an energetic propellant has already been demonstrated to significantly improve the mode of operation of the microthruster by increasing the coupling coefficient, thrust, ablation efficiency and specific impulse, we consider in this chapter the construction of a slightly different propellant tape strip with arranged 'cups' of energetic propellant. Whereas in previous experimental ventures the laser energy was intentionally held low enough to avoid any uncontrolled detonation [8], in this investigation, the material is intentionally detonated. The cup provides a rigid support that would stop detonation from occurring any further; this would offer a new mode of operation that would afford a higher coupling coefficient and thrust without much change to the laser parameters, as will be shown. However, attention must be paid to the modeling characteristics of the propellant as a chemical material, and to the detonation properties of the propellant. To this purpose, the MACH2 detonation module was implemented in this computational model. Below we further explore the implications of properly modeling an energetic propellant in MACH2 and discuss the computational model constructed; an analysis and presentation of the results follow.

4.2 Previous Experimental Work with Energetic Propellants

Numerous experimental tests have been performed that directly investigate influence of the coupling coefficient, specific impulse and thrust associated with exothermic compounds [1, 8, 14–16]. Polyvinylchloride or some close variant is usually tested in every experiment as a baseline passive solid target for comparison. A diversity of energetic materials have been explored; the experimental values determined from several previous experiments are reported in Table 4.1. The values vary widely due to very different testing conditions; however, general trends may be revealed by their comparison.

In more recent research (since 2007, [1,16]), two competing designs of the microthruster have come to emerge; in the first, specific impulse is emphasized as the critical performance factor, and passive solid targets are used (now referred to as the nsμLPT design), while the newer design (termed the msμLPT) operates for maximal coupling coefficient by implementing the exothermic propellant target [1]. Even newer designs [16] have advocated a compromising design wherein the thruster may operate in different modes by changing laser parameters.

4.3 Propagation Plasma Detonations in the Thruster

While laser-supported combustion is a favorable condition for the operation of the microthruster with an energetic propellant, laser-supported detonation would be disastrous to its operation. The initiation of a shock in an exothermic propellant could induce laser-supported detonation, allowing the propellant fuel tape to detonate in an uncontrolled fashion [8]. It is therefore a significant design consideration as to whether or not a detonation could occur due to the ablation. Theoretical work regarding the microthruster has been performed [8] to demonstrate that the ablation pressure does not exceed the threshold pressure at which a detonation would occur. We can describe the shock formation by the relationship

$$\nabla p = \rho v \cdot \nabla v \tag{4.1}$$

from which results the usual solution,

$$p = \rho v^2 = \rho {c_s}^2 \tag{4.2}$$

Using typical values from literature regarding the material [8], we consider for brevity of proof the acoustic speed of the material to be

$$c_s \approx 1\mathrm{km/s} \tag{4.3}$$

and mass density to be

$$\rho \approx 1000\mathrm{kg/m^3} \tag{4.4}$$

From the above relation, we have a threshold pressure for a propagating detonation to occur at $1 \cdot 10^9 \mathrm{N/m^2}$. We can relate this to the energy density of the material, given by

$$u = \frac{3}{2} nkT \tag{4.5}$$

If we consider the shock expansion wave as a perfect gas,

$$u = \frac{3}{2}p = 1.5 \cdot 10^9 \mathrm{J/m^3} \tag{4.6}$$

The laser-induced ablation pressure may be further related to the coupling coefficient and laser intensity as [8]

$$p = C_m I \tag{4.7}$$

In the experimental work, pressures of no higher than $10^5 \mathrm{N/m^2}$ were observed, and no laser-supported detonation resulted.

Previous experimental work has already demonstrated a sub-detonation-pressure scenario of micro-thruster operation [1, 13–16], which has indeed shown vast improvement of the coupling coefficient. The C_m for the passive solid propellant of 200N/MW improves to around 3,000N/MW for glycidyl azide polymer fuels. This would be useful in higher-thrust micro-thruster missions. Laser-supported detonation is typically avoided due to the disastrous results of an uncontrolled propagation through the fuel tape. However, if the fuel tape could be redesigned as to allow laser-supported detonation without the uncontrolled shock through the rest of the fuel, a laser-supported detonation would allow significantly higher thrusts to be attained. That is the purpose of the energetics simulation presented in this thesis, to demonstrate a higher level of thrust via a laser-supported detonation, rather than using sub-detonation-pressure operation. This is further warranted due to recent interest in the development of a multinewton micro-thruster mode of operation [16]; the experiments aim to achieve 6N of total thrust.

4.4 Construction of a Computational Model

From the previous experimental work, it is clear that glycidyl azide polymers and polyvinylnitrates provide the optimal performance properties. Glycidyl azide polymer demonstrates an enormous laser momentum coupling coefficient, allowing more thrust to be achieved, while polyvinylnitrates tend to provide much larger specific impulses. Since in Chapter 2 we have already shown that these two properties cannot be arbitrary, this is expected. This is where the microthruster design has recently split into the two separate designs of the nsμLPT and the msμLPT, the former optimizing specific impulse and the latter concentrating on larger thrust [1].

Two primary computational models were constructed, representing material approximations of glycidyl azide POLYOL (as used in the experimental work) and HMX-based plastic binding explosive PBX9501. Glycidyl azide polymer was chosen due to its optimal performance in experiments; PBX9501 was selected due to available material properties for appropriate modeling. Literature regarding the glycidyl azide polymer fuel [32] has already indicated a new energetic composite material propellant based on a mixture of glycidyl azide and HMX; therefore, a computational model of both is of interest. The HMX material was tested primarily as a means of verifying the computational model and Mach2 operation, and will not be presented here because the boundary conditions considered for this simulation do not cohere with the simulation purpose. The glycidyl azide test was performed with proper boundary conditions as for a wall structure present on the sides of the fuel tape, a simple means of allowing for laser-supported detonation without an uncontrolled shock propagating through the rest of the fuel.

The glycidyl azide model was developed as a means of investigating thrust levels achievable by intentional laser-supported detonation of the fuel, which has been previous unexplored in experimental work. Detonation of the energetic material has been avoided because it could introduce propagation of a detonation through the entire fuel tape. However, if a concept were implemented to stop an uncontrolled propagation by redesigning the fuel tape, it is of interest to see what improvements would be attainable by direct detonation. Therefore, in this simulation model, the ablation pressure was higher than the threshold pressure of detonation. The detonation releases a much larger mass ejection and achieves higher thrust. The boundaries of the fuel tape in the computational domain were designed as walls, since deposition techniques could be used to construct walls for 'cells' of single-shot explosive thrust along the fuel tape. This would make the fuel tape akin to an ammunition strip, where every cell of glycidyl azide represented a single thrust quantum attainable; the walls would have to be constructed to stop any uncontrolled detonation from traveling to the rest of the fuel. It is not the purpose of this simulation to investigate the wall design; that must be a future consideration. Instead, we focus on the large achievable thrust available to such a detonation. The cell ablation setup is shown in Figure 4.1,

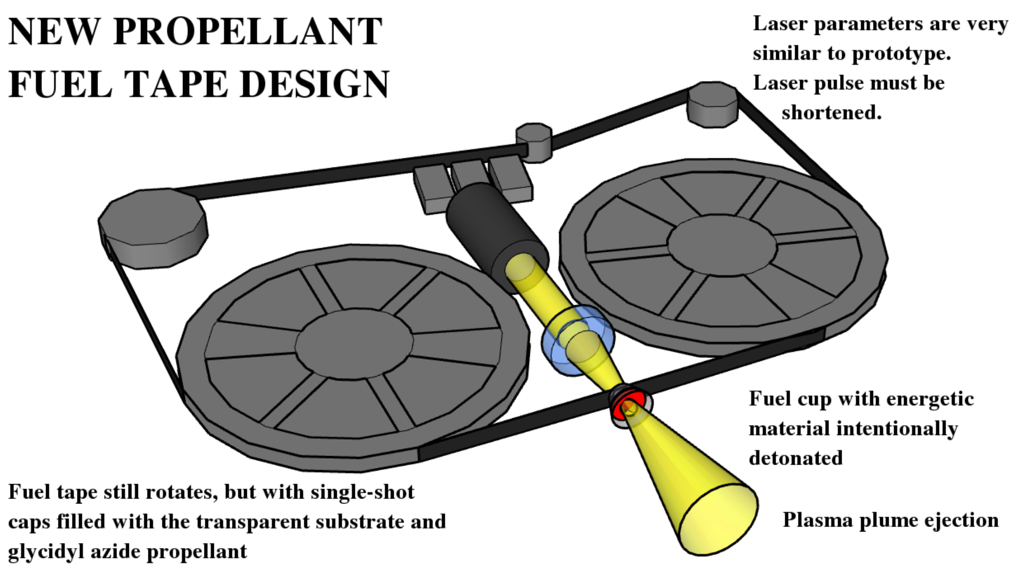

Figure 4.1: Design concept for 'cups' of propellant. Multiple cups along strip not shown. Transmission-mode ablation is implemented.

and the transmission-mode microthruster operation for this cell can be seen in Figure 4.2. For the simulation presented, the laser pulse duration would need to be shortened to the microsecond regime; however, the nsμLPT design has already demonstrated laser power in the nanosecond regime, so this is considered a feasible design for micro-thruster operation with the current technology of the prototype.

In order to implement the ammunition strip idea for the fuel tape, all that is needed is to instruct MACH2 to treat the walls bounding the propellant radially as rigid and impassible (in the previous simulations these propellant boundaries were set to keep their initial values of pressure and mass flow.) The physical properties necessary for a simulation of GAP and HMX are presented in Table 4.2. The decomposition temperature was used to approximate a rough specific internal energy at which detonation would occur; this threshold is presented in Table 4.2. The energy released upon detonation was measured previously and its value is used here [15]. The propellant modeled is essentially a GAP/HMX mixture of properties; however, for a proof of concept, this properly demonstrates the achievable thrust levels for a detonation. Future simulations can use different material properties.

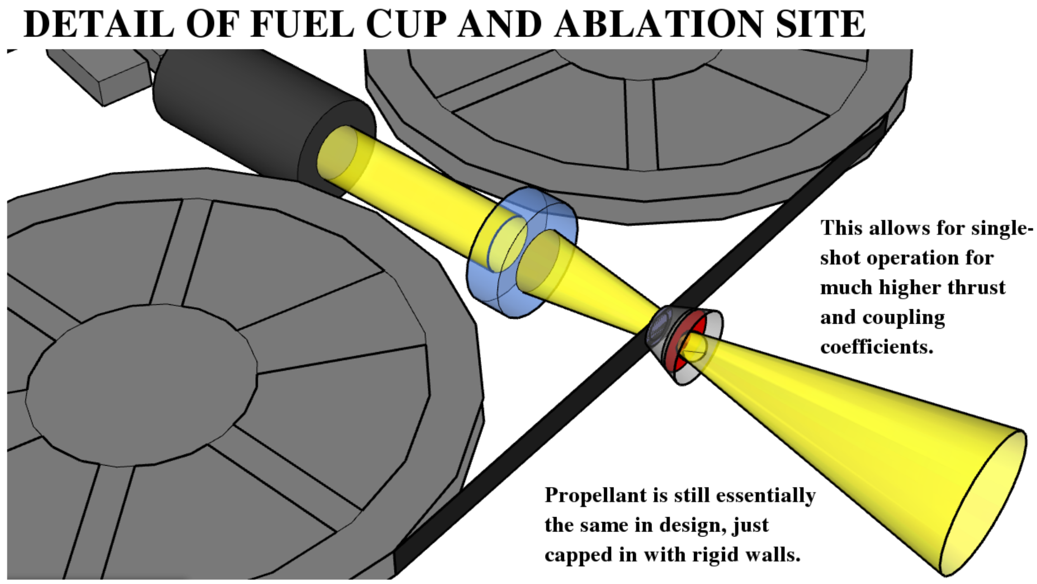

Figure 4.2: Detail of the design concept for the laser ablation of the cup. The cup walls are rigid and stop uncontrolled detonation, but allow intentional laser-supported detonation of propellant for higher thrust.

Table 4.2: Properties of the simulated ablatant propellant with energetic properties.

Physical Properties of GAP and HMX			
	Density kg/m^3	Detonation Threshold MJ/kg	Detonation Energy MJ/kg
Glycidyl Azide POLYOL	1,290	22	2.5
PBX9501 (HMX explosive)	1,840	3.5	5.54

4.5 Simulation Results

The simulation results for the glycidyl azide test are shown as a two-dimensional axisymmetric pseudocolor contour plot of density in Figure 4.3, where the physical configuration of the GAP polymer fuel can be seen for times from 0.1 to 1.0 microseconds. Results of the simulation are presented in Table 4.3. Detonation is achieved at around 0.4μs, which initiates an explosive reaction of the fuel. Speeds of the exiting plume were shown during the simulation to reach as high as 50km/s. Average exhaust velocities were around 10km/s. Using the methodology described in Chapter 3, a large ejected mass was determined (on

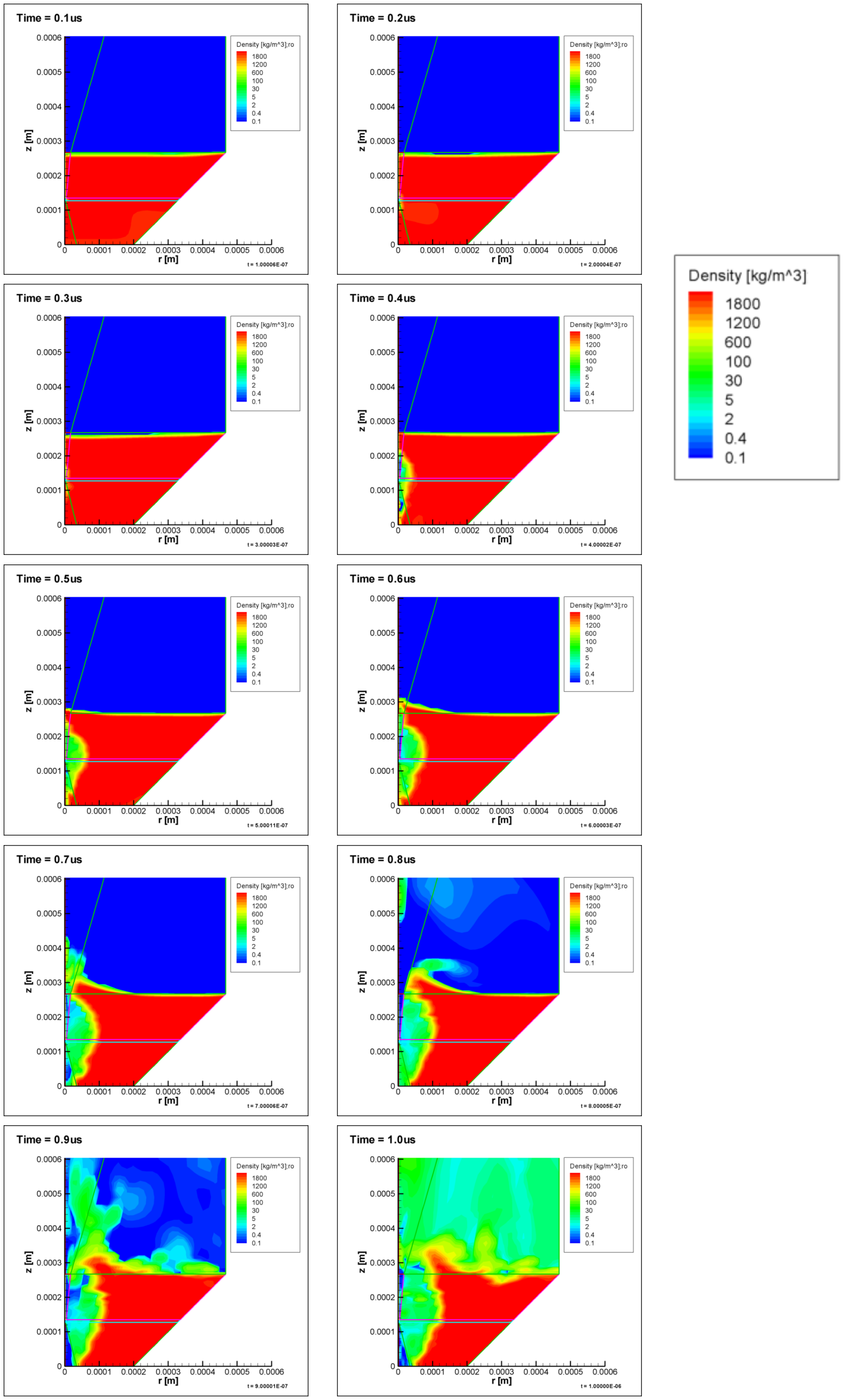

Figure 4.3: Energetics simulation density results for glycidyl azide polymer (GAP) propellant, for simulation times of 0.1 to 1.0 microseconds.

Table 4.3: Results from the Energetics Simulations performed in MACH2. [1] means predicted performance.

Results from the Energetic Simulations performed in MACH2			
	Baseline [2]	Energetics	Experimental [1, 3, 8, 12, 14, 15]
Simulation time, [μs]	0.67	1.58	—
Mass ejected, [ng]	0.600	1.853	0.400[1]
Avg. Laser Power, [W]	1000		4–15
Avg. Thrust, [mN]	830	4,502	10mN–1N
Impulse Bit, [μNs]	3.33	7.36	0.05
Avg. Exhaust Velocity, [m/s]	2,439	3,970	2,500
Coupling Coefficient C_m, [N/MW]	1,664	367,770	3,000
Specific Impulse I_{sp}, [s]	250	397	250
Ablation Efficiency, η_{ab}, [%]	9.1	401	198

the order of nanograms, an order of magnitude higher than experimental cases), and hence a large momentum was generated. Table 4.3 offers a comparison of the simulation results to the baseline 2mJ test and to experimentally-determined data.

All of the results presented in Table 4.3 are for the glycidyl azide test. The coupling coefficient is much larger than either the computational baseline or previous experimental work, indicating that an intentional detonation of the material could vastly improve microthruster performance for higher-thrust missions. Due to the enormous chemical energy released by the explosion, the ablation efficiency is also much larger (approximately 200% higher than experimental cases.) Because ablation efficiency essentially couples the laser momentum coupling coefficient C_m and the specific impulse I_{sp}, the specific impulse is also much larger. Despite the seeming disparity in this result, this still maintains the proper inverse relationship between C_m and I_{sp}, because of the much larger ablation efficiency.

Chapter 5

Introduction of an Axisymmetric Nozzle

5.1 Investigations of Adding an Axisymmetric Nozzle

One of the proposed means of improving thrust efficiency explored in these investigations considers the addition of an axisymmetric nozzle. The nozzle allows additional expansion of the released plasma, exciting thermal means of improving the propulsion. The addition of a nozzle to the microthruster design has already been proposed in the previous literature [33]; experimental investigations have already been made to determine certain characteristic trends [33]. However, the computational modeling of these nozzles allows for a more insightful study of the design parameters concerning the optimal nozzle design, as an experimental investigation would be costly and more difficult to ascertain. Computational investigations provide the benefit of being able to examine behavior and dependencies without the fabrication time and difficulty, cost and more complicated uncertainty of an experiment. If the Mach2 code can successfully demonstrate the proper physics regarding the microplasma expansion and can be shown to be 'calibrated' to a known baseline test, the determination of an optimal nozzle design can be explored and compared with more detail to the intricate dependencies on different design parameters. To this end, a computational investigation would serve to aid in the design of the nozzle and in the understanding of the theoretical influences occurring during thruster operation more easily than an experimental investigation would. After design trends and the investigations of different physics occurring in the thruster are evaluated, an experimental demonstration of the nozzle would become appropriate.

In the simulations made here, we are interested in demonstrating that the addition of a nozzle would indeed provide an improvement to the coupling coefficient, specific impulse and thrust; simulation results are presented that demonstrate corresponding trends to those already discovered experimentally in literature. This demonstration will be considered a proof of concept; the previous simulations performed in Mach2 for the study of laser plasma microthruster operation will be used as the baseline model of performance for the microthruster without any nozzle or design changes. We use the simulations performed to pursue a brief investigation of some of the design parameters concerning the nozzle. Methodology of data collection and analysis will be presented, and a comparison of results will be revealed at the end of the chapter.

5.2 Nozzle Design and Theoretical Considerations

A nozzle is designed to accelerate a flow; since this increases the momentum of the ejected mass, it increases the corresponding thrust force associated with the thrust operation. Nozzle designs are very dependent on the flow conditions of the exiting mass. It is well known [11] that the Mach number and thermodynamic states of the thruster chamber and nozzle influence the effect of the nozzle shaping the flow. Since the plasma expanding in the microthruster exhibits strong gas properties, we will consider briefly the typical nozzle theory.

Most treatments of nozzle theory consider the following assumptions valid to describe the flow adequately [11]:

(i) The propellant can be considered homogeneous and invariant

(ii) The substance obeys the perfect gas equation of state

(iii) No friction is present

(iv) No heat transfer occurs across the rocket walls (adiabatic flow assumption)

(v) Propellant flow is steady and constant, and no shock is present; no transient effects are present

(vi) All exhaust gases leave in an axially directed velocity

(vii) Flow velocity, pressure, temperature and density are uniform across the normal to the nozzle axis

(viii) Chemical equilibrium is established and maintained throughout the flow ejection

(ix) All species are gaseous

Only assumptions *(ii)*, *(vi)* and *(ix)* can be asserted with any certainty regarding the plasma plume in the microthruster. All other assumptions are questionable at best. Because the MACH2 code will simulate more rigorous physics regarding the plasma expansion, the typical nozzle theory will probably not be particularly well-suited for designing the nozzle here. However, as a means of simply qualitative investigation, it will at least provide guidelines for the construction of a nozzle model.

The nozzle shape is determined by the Mach number of the gas flow. The differential equation describing the relation between the rate of the nozzle area and velocity of flow projected along the nozzle axis is given as [11]:

$$\left(\frac{u^2}{a^2} - 1\right)\frac{du}{dx} = \frac{1}{A}\frac{dA}{dx} \tag{5.1}$$

Here a is the acoustic speed of the propellant gas, the speed at which sound waves propagate, given by

$$a = \sqrt{\frac{c_p}{c_v}RT} \tag{5.2}$$

We can clearly see from the differential equation above that when the gas flow velocity u is less than the acoustic speed a, the left-hand side is less than zero, so the rate $\frac{dA}{dx}$ must be negative; this indicates that the nozzle shape must *converge* for subsonic flows. This converging shape will accelerate the flow by diminishing the area. At the critical point where Mach 1 is achieved, the left-hand side becomes zero, and the area must remain constant in this small region. When the gas flow has overtaken the acoustic speed, the left-hand side is inherently positive, indicating that the nozzle area rate $\frac{dA}{dx}$ must increase; this means the nozzle must *diverge* in order to accelerate a supersonic flow.

Typical rocket nozzles introduce a converging and diverging staged nozzle design behind the thruster. The converging section accelerates the subsonic combusted gas expansion to Mach 1, where the diverging nozzle shape begins. This allows supersonic expansion of the gas out of the spacecraft. However, by investigation of the velocity components projected along the nozzle axis (in the z-direction of the simulation coordinate system) from the previous computational model of the solid-propellant microthruster operation and from experimental measurements, the plasma plume velocities are on the order of 1-2km/s. Furthermore, the literature [8] also indicates that the measured exhaust velocities are supersonic compared to the typical acoustic speed of the propellant (which is usually taken to be $c_s \approx 1$km/s [8]). This indicates that the plasma is already supersonic just after ablation; therefore, a subsonic converging nozzle would be unnecessary and actually detrimental to the flow. In the construction of a computational model for the microthruster simulation, only diverging nozzle shapes were considered.

The ideal nozzle design begins with a high pressure, high temperature flow within the chamber, and allows the flow to expand until it reaches the end of the nozzle, where the flow pressure matches the ambient pressure of the environment. A difference in flow pressure and ambient pressure at the nozzle exit can introduce significant problems to the exit flow. A nozzle that discharges the flow at a pressure greater than the external pressure is termed an *underexpanding* nozzle, and exhibits a sudden large waist bulge of fluid at the nozzle exit. In contro, a nozzle wherein the flow pressure is less than the external pressure is called *overexpanding*, and exhibits a tapering of the plume tail well before the end of the nozzle. Such design problems result from incorrect nozzle area expansion ratios, and must be evaluated and considered before a proper nozzle design may be implemented. Due to the complexity of the physics simulated by the MACH2 code, the nozzle expansion ratio cannot be simply calculated, so the simulation was rerun with different lengths to suggest an optimal length which allows for proper expansion.

There exists a variety of diverging nozzle shapes, each usually designed for a specific purpose in mind. However, most of these nozzle designs emerged as results of the above assumptions applied to rocket flow. Since it is uncertain *a priori* if most of these assumptions apply at all, the flat conical nozzle shape and the contoured (or bell) nozzle shape were selected for computational modeling. Due to the uncertain nature of the physics of the expansion process beforehand, it is unclear beforehand if these nozzle shapes will perform as expected for typical rocket flows. To this end, it is the purpose of these investigations to validate any advantage of one design over the other. Simulations were executed for both of these designs; however, designs in geometry focused on contoured shapes, since these are generalized cases for simulation of conical nozzles.

5.3 Construction of a Computational Model

The initial simulation was re-executed for the 2mJ case; however, due to an unexpectedly large mass being ejected (the simulation was noted to have been an order of magnitude in predictions higher than experimental results [2]), a new baseline was designed for this situation. Since we want to compare the effects of simple ablation with no nozzle present, the original simulation was modified to include a 210-micrometer-thick wall covered the propellant except for a 50-micrometer-diameter bore aligned with the axis of symmetry. Although somewhat artificial, this serves as a good base for comparison with the nozzle case because the same amount of mass is ejected, but no nozzle effects are present (the wall is essentially a zero-half-angle nozzle, introducing no expansion effects aside from what occur after having passed through the bore). Pseudocolor density contour plots of this baseline are displayed in Figure 5.1. The numerical results postprocessed using the methodology described in Chapter 3 are included in the simulation results in Table 5.1.

Since it is desirable to at least confirm general nozzle trends as expected, six data points were examined: two different nozzle lengths with three half-angle tests each. This allows a brief examination of the trends regarding nozzle length and nozzle half-angle. It is expected that with increasing half-angle and increasing length, there would be a continuous increase of the coupling coefficient due to more allowed expansion of the fluid. This is not completely true; clearly, there will be a critical point past which the expansion will disappear back to a typical bored hole (baseline), and similarly an infinitely-long nozzle will introduce a large addition of mass to the thruster. However, for the intentions made clear in our objective, this examination suffices; it is left to future work to determine an optimal angle

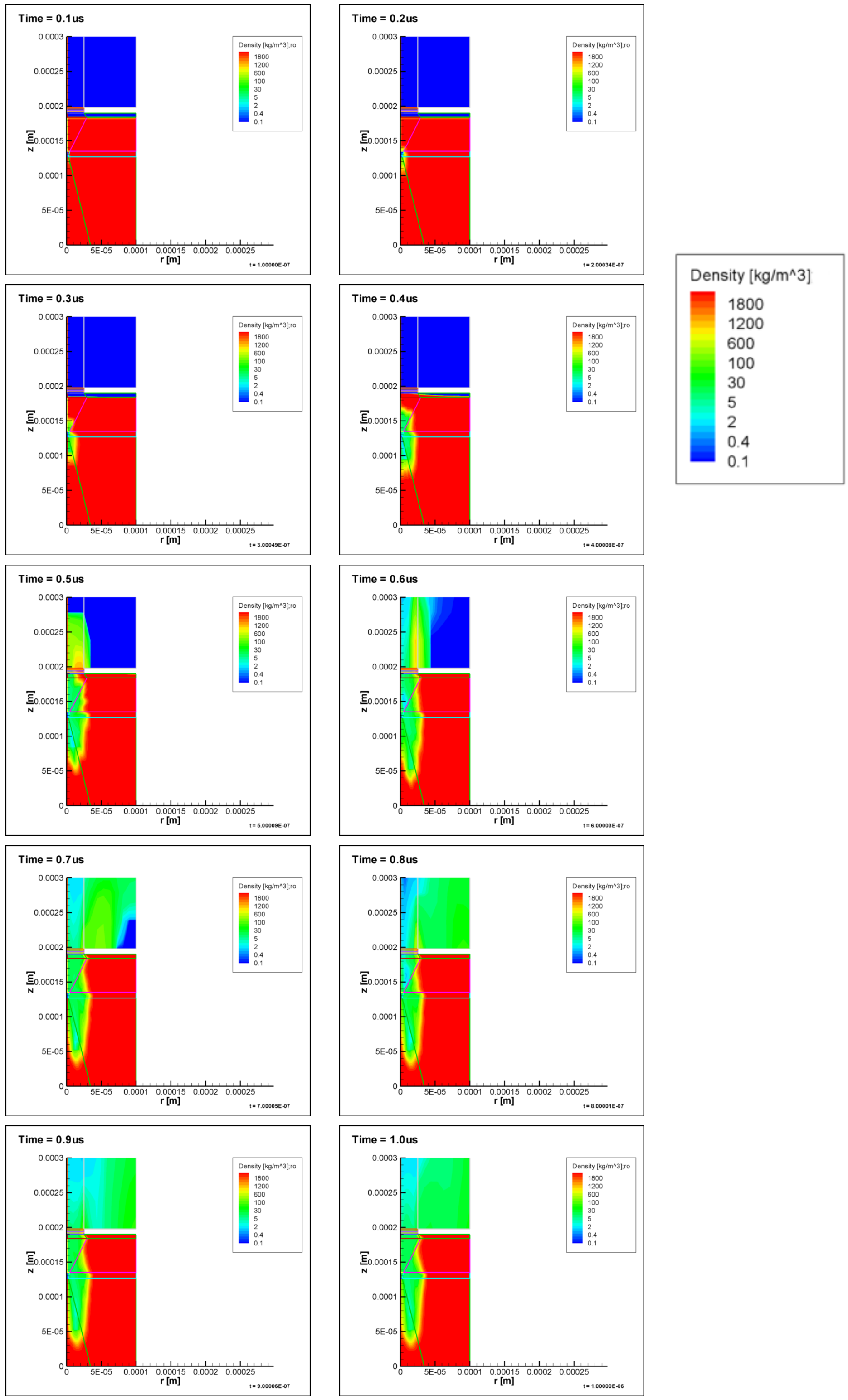

Figure 5.1: Density contour plots of the nozzle-prepared calibration; 210-μm-length zero-half-angle bore hole. Shown for 0.1 to 1.0 microseconds.

Table 5.1: Results from the Contoured nozzle simulations performed in MACH2.

Contoured Nozzle Design Simulation Results							
	Baseline	210μm-length Nozzles			90μm-length Nozzles		
Nozzle Type (see Fig 5.2):	15	21	23	24	27	28	29
Parameters:	0°-half-angle	12°	20°	25°	12°	15°	20°
Simulation Time, [μs]	0.67	1.07	1.96	2.68	1.67	0.72	1.67
Mass Ejected, [ng]	0.600	0.477	0.452	0.381	0.434	0.417	0.517
Avg. Thrust, [mN]	269	311	403	409	446	498	366
Impulse Bit, [μNs]	0.190	0.336	0.795	1.104	0.748	—	0.616
Exhaust Velocity, [m/s]	316	703	1,760	2,898	1,722	13.3	1,192
C_m, [N/MW]	95	168	398	552	374	2.77	308
I_{sp}, [s]	32	70	176	290	172	0.13	120
η_{ab}, [%]	1.7	5.6	35	80	32	0	18.4

of operation or length (which would depend as well on mass of the nozzle material, which is undetermined at this point).

The geometries tested are shown in Figure 5.2. The propellant tape is simulated in a very similar respect to Blocks 1 through 6 of the original simulations. An air gap between the nozzle and the tape was included for the purpose of a more realistic simulation; this distance was approximately six microns. The nozzle was approximated in a contoured fashion with four 'stages', each bent at a slighter angle than the preceeding stage. The lengths explored corresponded to 210μm and 90μm. Half-angles between 12° and 25° were investigated. The nozzle designs were numbered and tested; the successful simulation executions are presented in the results that follow.

5.4 Simulation Results

Six successful simulations demonstrated trends for nozzle characteristics. The first set, for the 210-μm length, shows a definite trend of increasing coupling coefficient with increasing half-angle. This complements known experimental data for nozzles (although there is eventually a critical half-angle at which nozzle performance becomes detrimental to the thruster performance). This indicates that a nozzle of around 200μm in length would effectively increase the performance of passive solid fuels. The 90-μm length equally shows improvement over the baseline consideration, but does not produce the same effective performance enhancement as the longer nozzle. These two data points of length indicate

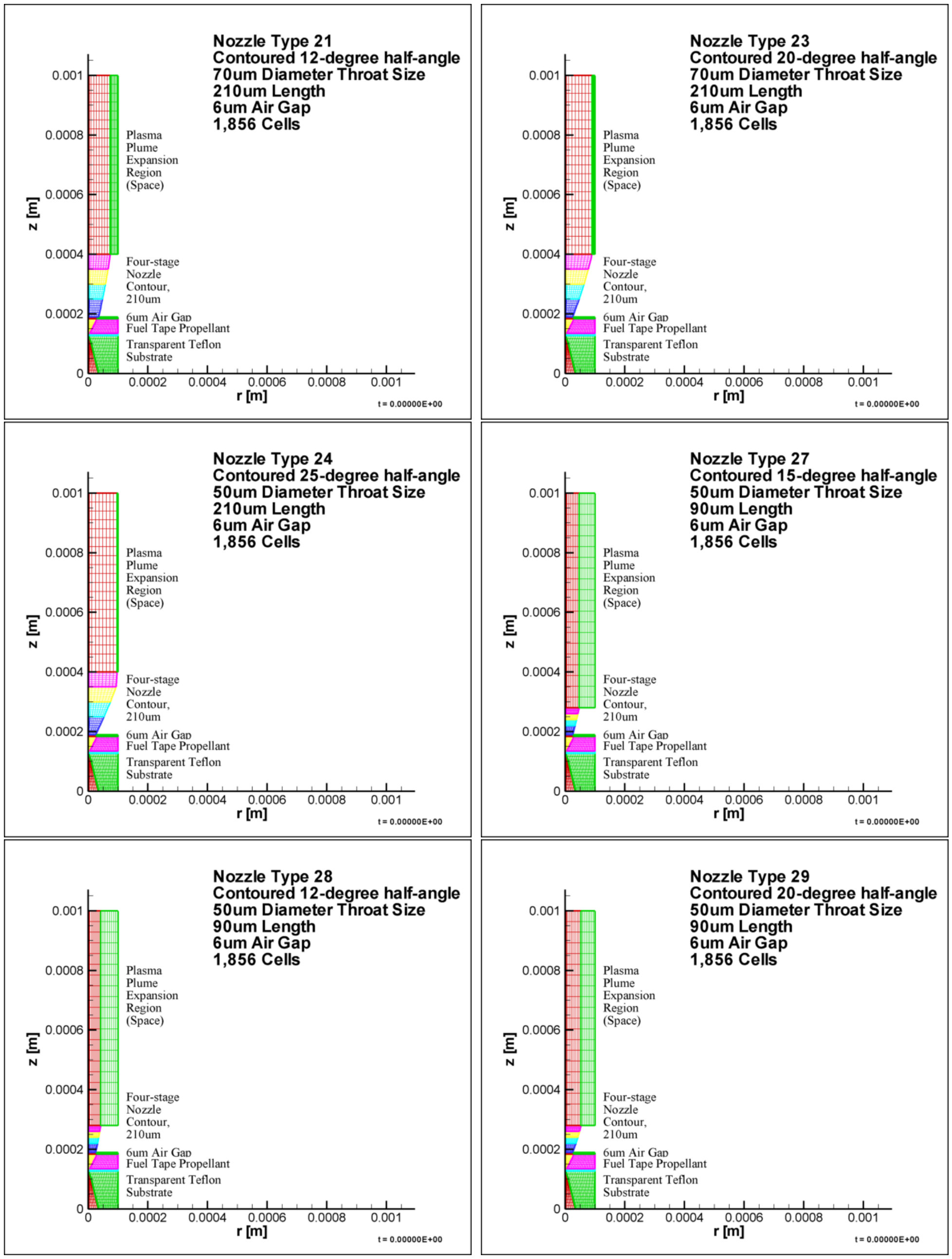

Figure 5.2: Geometries implemented for the Mach2 nozzle simulations.

that the longer nozzle design was more successful, so a nozzle with a length around 200μm should be considered for improvement of the propellant.

It is also important to consider the choking point of the propellant. The previous 2mJ simulation [2] was not representative of a realistic design due to the large mass ejection (which does not correspond to experiment), but placing the nozzle wall over the propellant stopped this ejection. This result is why a different calibration was needed for simulation comparisons, as discussed above.

An increase in both I_{sp} and C_m could be somewhat unexpected, since these two parameters are intrinsically related to each other in an inverse fashion, but because the nozzle improved the overall ablation efficiency (at least, strictly in a mathematical sense), more specific impulse and coupling coefficient were accessible to the micro-thruster. This demonstration of increasing available ablation efficiency, and hence increasing both coupling coefficient and specific impulse, was observed experimentally as well [34]. The nozzle tests performed indicate that coupling coefficient and specific impulse increase with increasing nozzle half-angle, and that a longer nozzle (around 210μm in length) is more appropriate for creating larger thrusts than a smaller (90μm) nozzle. The nozzles were not tested for heat transfer effects or for durability; such features must be considered in any successful nozzle design; however, any study of such problems is beyond the scope of this thesis. The best scenario simulated offers an increase of 457N/MW for the coupling coefficient over the experimental results. This is about a 230% increase compared to experimental data. Gains in specific impulse are hard to assign exact values, due to the instantaneous nature of the measurement and the difficulty in selecting a consistent measurement technique for comparison with experimental values; however, the presence of an increased ablation efficiency clearly indicates that more specific impulse is accessible and expected for such situations. The physical results of the six simulations are presented as two-dimensinal axisymmetric pseudocolor contour plots of density in Figures 5.3–8, respectively, for the 210μm-length 12, 20, and 25 degree cases, and the 90μm-length 15, 12, and 20 degree cases, respectively; these graphs are presented to illustrate what is happening in physical space during the ablation process. The high-density regions are solid, while the low-density regions are plasma plume escaping from the ablation process; the blue background corresponds to the background gas present in the simulation (air at 5mtorr).

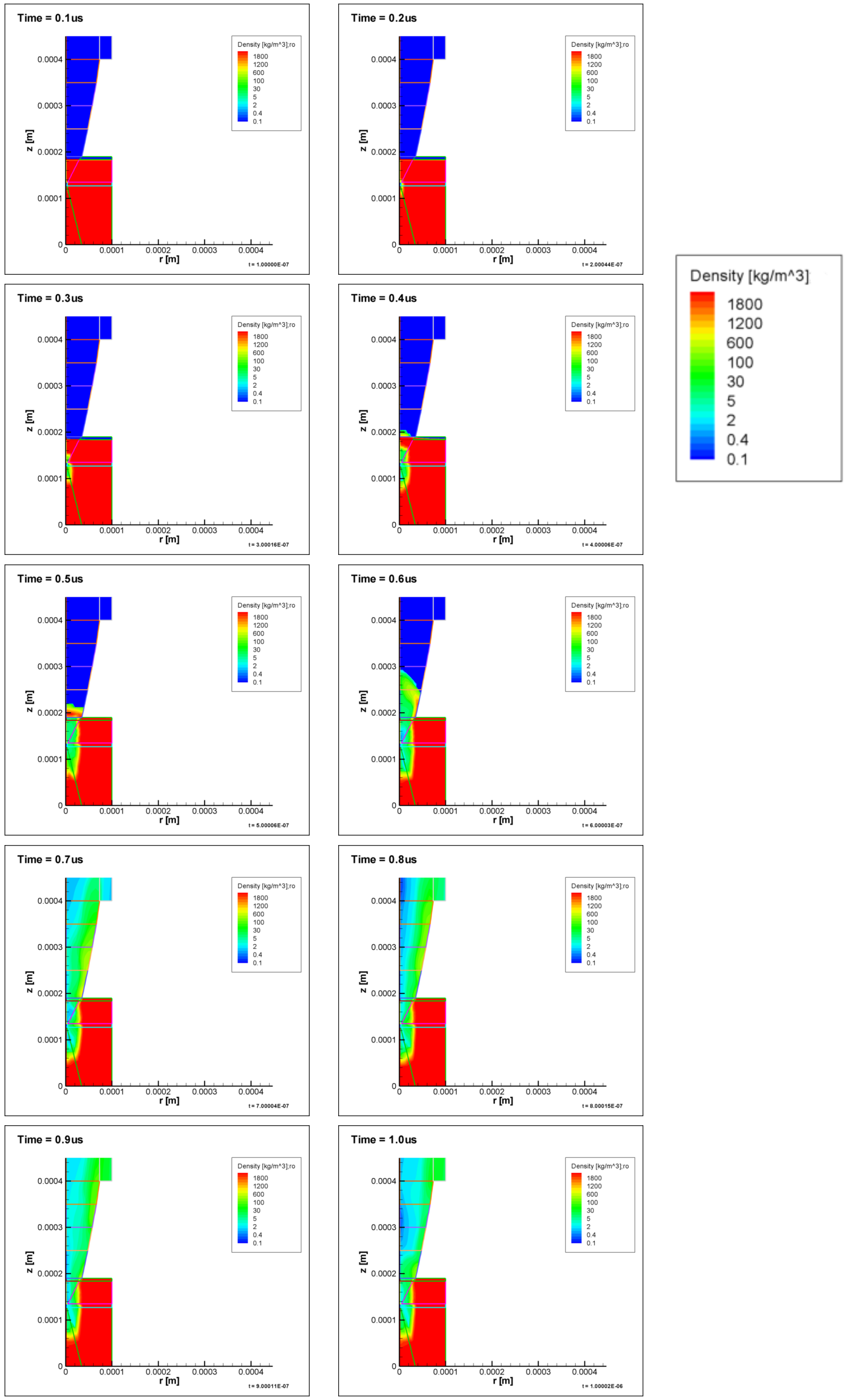

Figure 5.3: Density contour plot results of simulation for Nozzle 21; 210-μm length, contoured stages of 12, 11, 10, and 8 degrees respectively; shown for 0.1 to 1.0 microseconds.

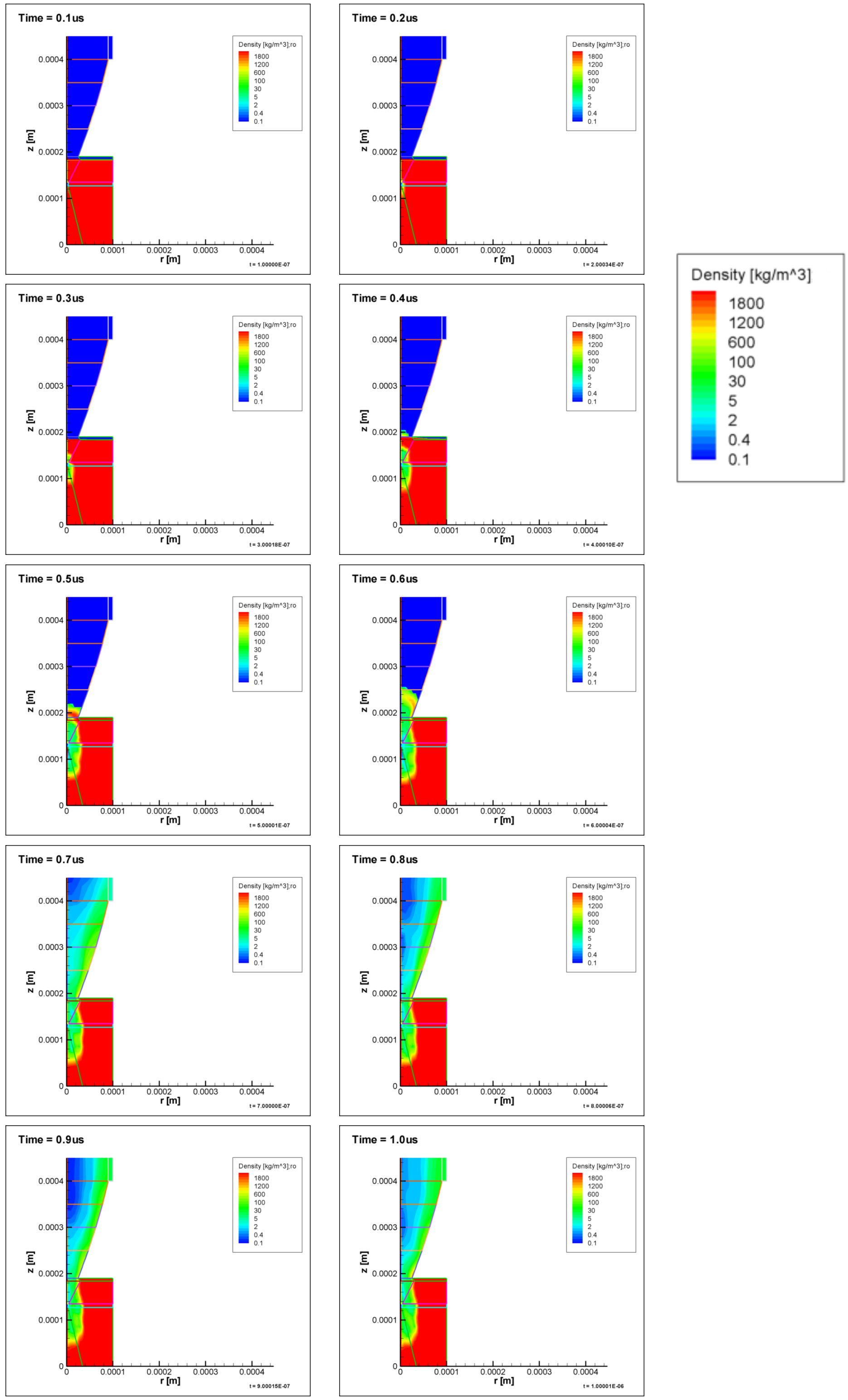

Figure 5.4: Density contour plot results of simulation for Nozzle 23; 210-μm length, contoured stages of 20, 18, 16 and 14 degrees respectively; shown for 0.1 to 1.0 microseconds.

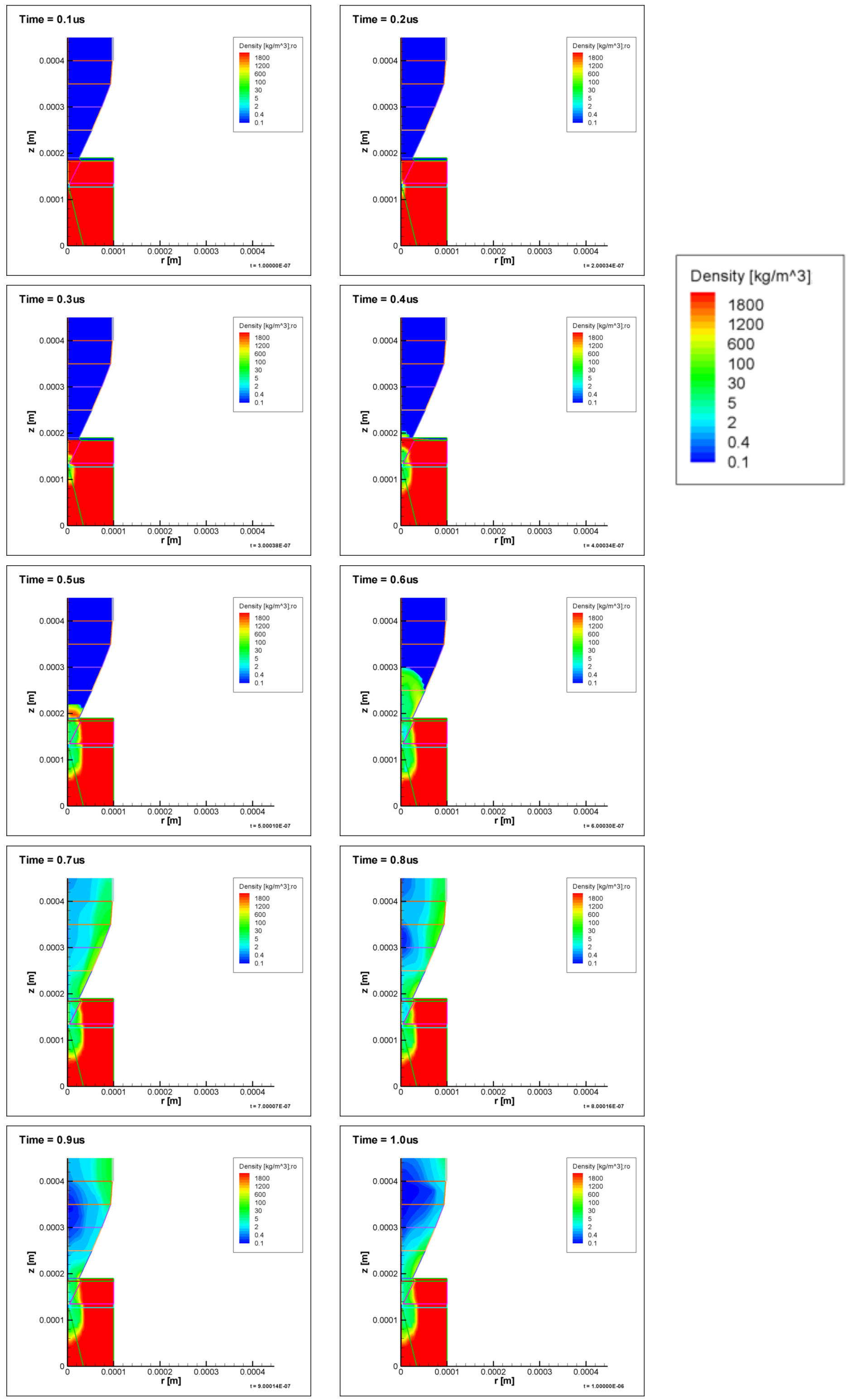

Figure 5.5: Density contour plot results of simulation for Nozzle 24; 210-μm length, contoured stages of 25, 23, 21 and 19 degrees respectively; shown for 0.1 to 1.0 microseconds.

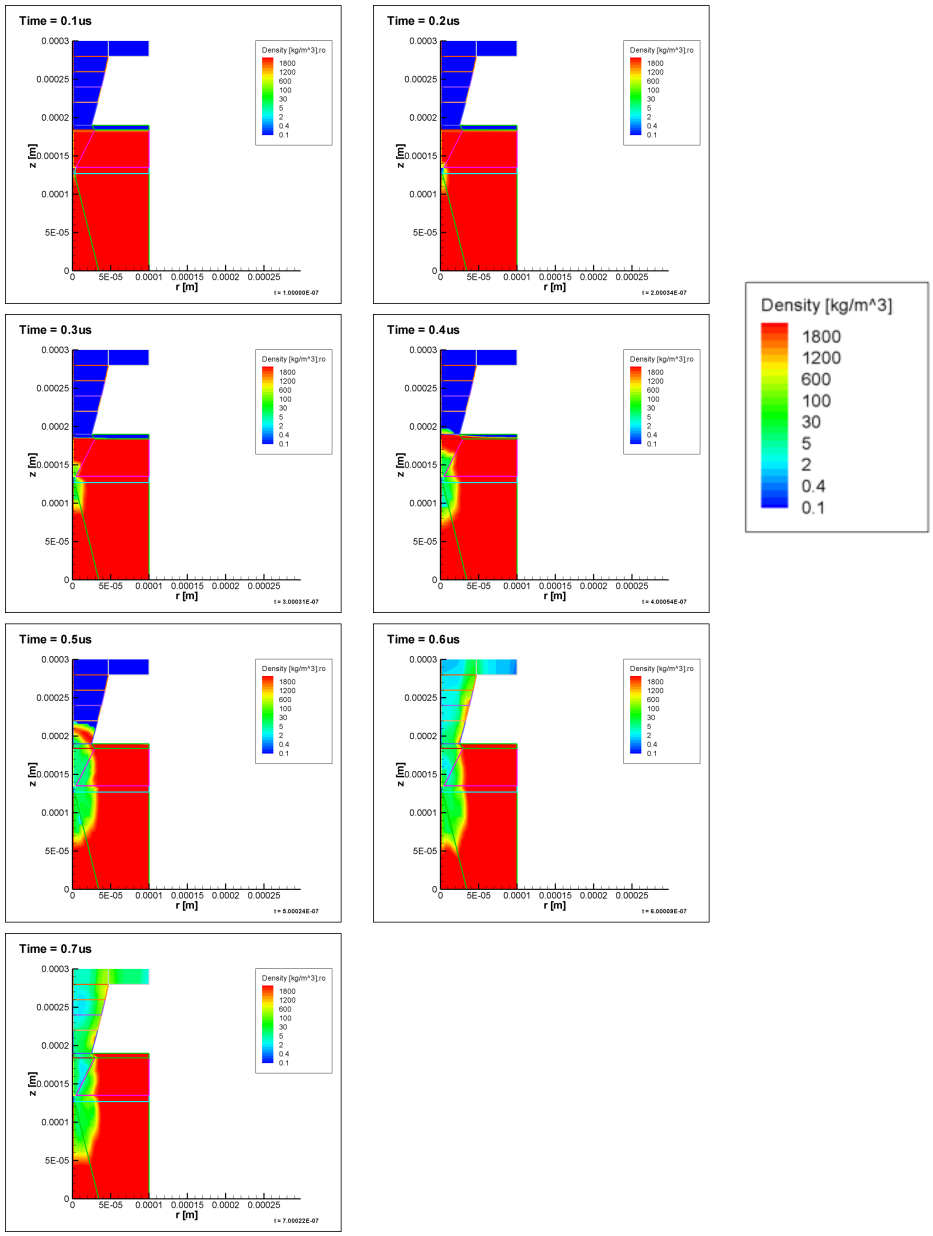

Figure 5.6: Density contour plot results of simulation for Nozzle 27; 90-μm length, contoured stages of 15, 14, 13, and 12 degrees respectively; shown for 0.1 to 0.7 microseconds (simulation ended.)

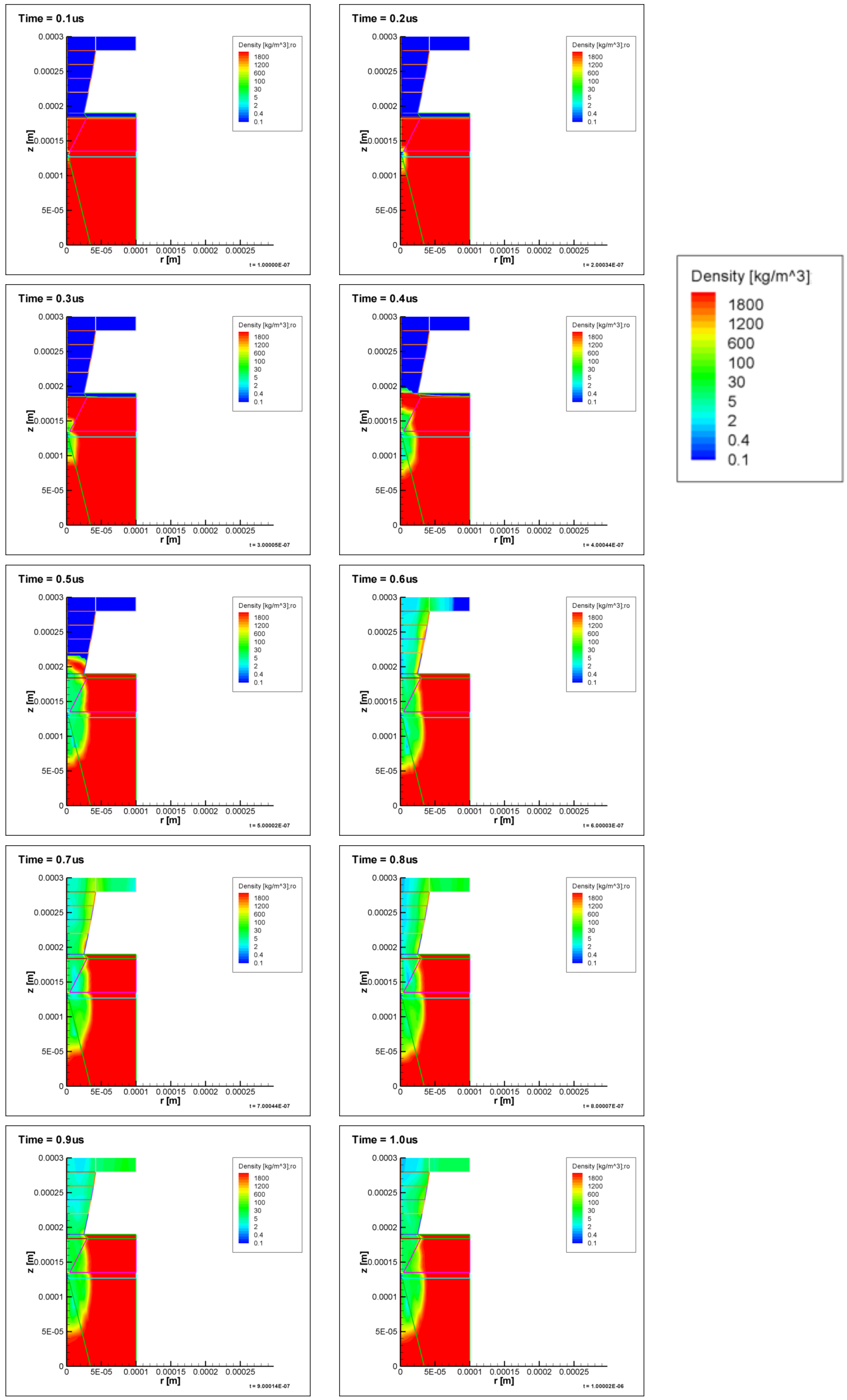

Figure 5.7: Density contour plot results of simulation for Nozzle 28; 90-μm length, contoured stages of 12, 11, 10, and 9 degrees respectively; shown for 0.1 to 1.0 microseconds.

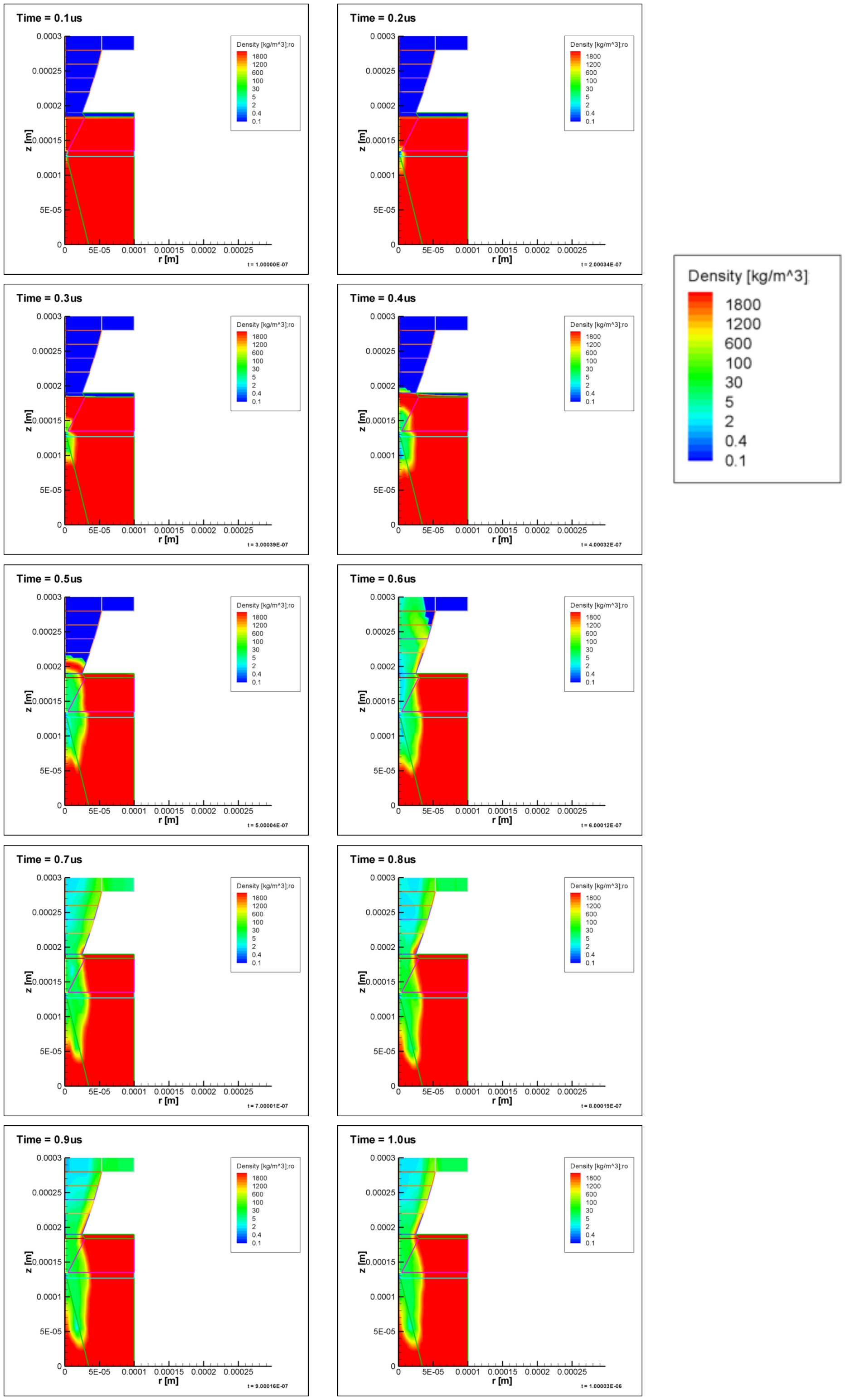

Figure 5.8: Density contour plot results of simulation for Nozzle 29; 90-μm length, contoured stages of 20, 18, 16, and 14 degrees respectively; shown for 0.1 to 1.0 microseconds.

Chapter 6

Conclusions and Future Work

6.1 Simulation Results and Trends

The following conclusions may be reached regarding the computational simulations presented here:

(i) Base computational work has been provided that demonstrates simulation of different micro-thruster modes of operation (axisymmetric nozzle and energetic propellant), and methodologies for evaluating the performance improvements have been presented;

(ii) Simulation of an intentional detonation of glycidyl azide polymer has been presented, which demonstrates enormous potential for improvement to the coupling coefficient C_m by almost two orders of magnitude, if the laser pulse duration is shortened;

(iii) Simulation of a set of three 210-μm-length nozzles has demonstrated expected trends for increasing the coupling coefficient of a solid, passive target compared to baselines and experiment, as long as the nozzle throat diameter is chosen carefully so as not to block to the escaping flow;

(iv) Simulation of a set of three 90-μm-length nozzles has also demonstrated an increase in performance over the baseline and experimental passive ablation, but was not as effective as a 210-μm-length nozzle.

The glycidyl azide polymer detonation mode of microthruster operation currently remains unexplored in experimental literature; previous work focuses on sub-detonation pressures for operation. Although these sub-detonation modes have demonstrated increased coupling coefficients, there is still potential for far greater improvements if the propellant can be intentionally detonated, as shown by these simulations. As described in Chapter 4, this would require modifications to the fuel tape design to stop an uncontrolled detonation, but this might be implemented by segmenting the fuel tape using deposition techniques. Furthermore, the laser parameters for the experimental case must be changed to achieve the same thrust simulated here; pulse durations on the order of microseconds were simulated here, however, it should be noted that previous experimental work with the nsμLPT has already demonstrated capable prototype technology in the nanosecond regime.

The nozzle simlations demonstrate that possible coupling coefficient improvements may be achieved by the introduction of properly-designed nozzles. Just as every rocket engine has a nozzle design to optimize its performance, these simulations have demonstrated that such an optimal arrangement exists. These simulations have not identified the optimal design. However, the typical nozzle trends demonstrated experimentally [34] and to be expected [11] have been shown to be the same for subkilogram laser micropropulsion for some nozzle designs, which indicates that the coupling coefficient can be greatly improved for solid passive propellants. Previous experimental work [35] has already been performed for the physical fabrication of nozzles on this scale, and these simulations provide work that may be used in future experiments to verify nozzle designs sufficient for substantial performance improvement of the micro-thruster operation. However, the physical nozzle parameters (half-angle, length, etc.) are also important, as also demonstrated; the nozzle must properly choke the flow in order that the best improvements be achieved.

6.2 Future Work

While these computational models provide a foothold into the proper simulation of the micro-thruster operation and also provide a tool for its design, there is a lot of room for improvement.

The detonation model would be better simulated if the deposited walls (which inhibit the propagation of a detonation wave) of the segmented fuel strip could be included and tested to withstand the detonation. It might also be of interest to test a computational domain simulating two fuel cells side-by-side with a wall, to see what changes are introduced to the neighboring cell. Dependencies of the coupling coefficient on laser fluence, waist and pulse duration could be tested by changing these laser parameters in Mach2 over a range of values and re-executing the model.

The nozzle models could be improved by testing for more dependencies than presented here; the nozzle performance enhancement with half-angle and length is critical to the proper design of a useful nozzle for laser micropropulsion. Different throat diameters and placements could also be tested. Different air gap distances could also be included to investigate the effects of the nozzle positioning vertically.

As of the current models, the nozzles could be further investigated for optimizing design parameters and investigating dependencies of laser parameters. The energetics model would need more consideration for the design of the segmented fuel tape before further simulation or propellant testing could ensue. Different energetic materials could also be evaluated for achieving higher thrusts, if material properties are available.

Another very interesting result of the simulations presented were oscillations of the thrust that occurred. It was observed in both nozzle and energetic cases. The thrust experienced large oscillations (the peak thrust rose an order of magnitude higher than its average), and after the mass ejection was complete, the oscillation had died down, and the average thrust was taken in these simulations. However, if any mechanism could be introduced that would take advantage of these oscillations and time the release of the bulk of the mass ejection for an outgoing oscillation, this could potentially improve the design considerations examined here. The energetics realized a peak thrust of 40N, yet its average was only 6.5N. By releasing the mass ejection at the peak of an oscillation, the thrust could possibly be increased by an order of magnitude. It is currently unknown how such a mechanism could be introduced to the micro-thruster; further, introducing it would increase the complexity of the thruster design as a whole.

Finally, a magnetic nozzle was also briefly considered. The complexity of the simulation precluded its inclusion in this thesis. A magnetic nozzle would be induced by a ring of current centered around the thruster axis providing long, vertical, solenoidal magnetic field lines; since the charged particles in the plasma respond well to magnetic fields, the particles would tend to follow the field lines rather than cross them. This could lead to a significant performance increase. The mass ejection seen in the previous computational work [2] shows much of the mass moving radially, which does not contribute to the thrust; with the presence of the field lines, the radial motion would be impeded and the fluid would move more along the thruster axis, augmenting the thrust. Investigations of the dependency of thruster performance on field strength could be tested with such a simulation. The MACH2 code is an adequate code for modeling such simulations because it uses hydromagnetics, so the electrodynamic equations are solved. In the simulations performed here, the magnetics were not required, so they were turned off; however, this MACH2 module would be useful for the simulation of a magnetic nozzle. The plasma detachment would be important in the design of a magnetic nozzle, because in some cases the plasma could follow the field lines to the spacecraft walls, not producing any thrust at all. Previous magnetic nozzle work [36] indicates that the flow must be superalfvenic in order for the plume to properly detach and break from the field lines. It remains to be seen if the microplasma produced by the μLPT here could be made superalfvenic within a reasonable solenoid length. Energy considerations of the current drawn for the generation of such a field must also be considered, since the available power of a micro- or nanosatellite would be very limited.

It is hoped that the investigations provided in this thesis will complement the extensive experimental investigations for micro-thruster design with new computational tools for performance enhancement investigation and design tools for determining critical and optimal design parameters for implementing such performance improvements. It is also hoped that this investigation introduces new design ideas for implementation and demonstrates the feasibility of both.

Bibliography

Bibliography

[1] C. R. Phipps, J. R. Luke, W. Helgeson, and R. Johnson, "Performance test results for the laser-powered microthruster," in *Beamed Energy Propulsion: Fourth International Symposium* (K. Komurasaki, T. Yabe, S. Uchida, and A. Sasoh, eds.), 2006.

[2] T. Moeller and Y.-K. Chang, "Mach2 simulations of a micro laser ablation plasma thruster," *Aerospace Science and Technology*, vol. 11, pp. 481–489, 2007.

[3] C. R. Phipps, J. R. Luke, G. G. McDuff, and T. Lippert, "Laser-driven micro-rocket," *Appl. Phys. A*, vol. 77, pp. 193–201, 2003.

[4] C. Phipps, J. Luke, and W. Helgeson, "Laser space propulsion overview," in *Proceedings of SPIE Vol. 6606* (D. Dumitras, M. Dinescu, and V. Konov, eds.), 2007.

[5] G. Marx, "Interstellar vehicle propelled by terrestrial laser beam," *Nature*, vol. 211, pp. 22–23, 1966.

[6] M. M. Michaelis, "Eugene sanger memorial," in *Proceedings of SPIE Vol. 3343*, 1998.

[7] M. A. Libeau, L. N. Myrabo, M. Filippelli, and J. McInerney, "Combined theoretical and experimental flight dynamics investigation of a laser-propelled vehicle," in *38th AIAA/ASME/SAE/ASEE Joint Propulsion Conference & Exhibit*, 2002.

[8] C. Phipps, J. Luke, T. Lippert, M. Hauer, and A. Wokaun, "Micropropulsion using a laser ablation jet," *Journal of Propulsion and Power*, vol. 20, no. 6, 2004.

[9] I. D. Boyd and M. Keidar, "Simulation of the plume generated by a micro laser-ablation plasma thruster," in *Proceedings of SPIE Vol. 4760* (C. R. Phipps, ed.), 2002.

[10] M. M. Michaelis and J. D. Hey, "Pioneers of laser propulsion Saenger, Marx, Moeckel and Kantrowitz," in *Proceedings of SPIE Vol. 4760* (C. R. Phipps, ed.), 2002.

[11] G. Sutton, *Rocket Propulsion Elements: An Introduction to the Engineering of Rockets.* John Wiley and Sons, 5th ed., 1986.

[12] C. Phipps, J. Luke, and T. Lippert, "Laser ablation of organic coatings as a basis for micropropulsion," *Thin Solid Films*, vol. 453, pp. 573–583, 2004.

[13] C. R. Phipps, J. R. Luke, W. D. Helgeson, D. Naud, M. Hiskey, L. Urech, T. Lippert, and A. Wokaun, "Giant momentum coupling coefficients from nanoscale laser-initiated exothermic compounds," in *41st AIAA/ASME/SAE/ASEE Joint Propulsion Conference and Exhibit*, 2007.

[14] L. Urech, T. Lippert, C. R. Phipps, and A. Wokaun, "Polymers as fuel for laser plasma thrusters A correlation of thrust with material and plasma properties by mass spectrometry," in *Proceedings of SPIE Vol. 6261* (C. R. Phipps, ed.), 2006.

[15] L. Urech, T. Lippert, C. R. Phipps, and A. Wokaun, "Polymers as fuel for laser-based microthrusters: An investigation of thrust, material, plasma and shockwave properties," *Applied Surface Science*, vol. 253, pp. 7646–7650, 2007.

[16] C. R. Phipps, J. R. Luke, and W. Helgeson, "Laser-powered, multi-newton thrust space engine with variable specific impulse," in *Proceedings of SPIE Vol. 7005* (C. R. Phipps, ed.), 2008.

[17] R. G. Jahn, *Physics of Electric Propulsion.* McGraw-Hill, Inc., 1968.

[18] F. S. Simmons, *Rocket Exhaust Plume Phenomenology.* The Aerospace Corporation, 2000.

[19] W. L. Kruer, *The Physics of Laser Plasma Interactions.* Frontiers in Physics, Addison-Wesley Publishing Company, 1988.

[20] G. W. Sutton and A. Sherman, *Engineering Magnetohydrodynamics.* McGraw-Hill Book Company, Inc., 1965.

[21] H. Motz, *The Physics of Laser Fusion.* Academic Press, 1979.

[22] R. Fardel, L. Urech, T. Lippert, C. Phipps, J. M. Fitz-Gerald, and A. Wokaun, "Laser ablation of energetic polymer solutions: Effect of viscosity and fluence on the splashing behavior," *Appl. Phys. A*, vol. 94, pp. 657–665, 2009.

[23] J. D. Jackson, *Classical Electrodynamics.* John Wiley & Sons, Inc., 1999.

[24] G. A. Simons and A. A. Pirri, "The fluid mechanics of pulsed laser propulsion," *Journal of Propulsion and Power*, vol. 15, 1977.

[25] R. E. P. Jr., M. H. Frese, and C. R. Sovinec, "Transport of magnetic flux in an arbitrary coordinate ALE code," *Journal of Computational Physics*, vol. 140, pp. 148–171, 1998.

[26] M. H. Frese, "Mission research corporation report AMRC-R-874," no. No. ADA 192285, 1992.

[27] J. U. Brackbill and W. E. Pracht *Journal of Computational Physics*, vol. 13, 1973.

[28] J. J. Watrous and M. H. Frese, "A dynamic explosive model for MACH2: With applications to magnetic flux compression generators," Tech. Rep. Contract Number 9-XT1-Q4340-1, Los Alamos National Laboratory (LANL), 1993.

[29] J. J. Watrous and M. H. Frese, "Application of MACH2 to explosive magnetic flux compression generators Improvements in detonation modeling," Tech. Rep. Contract Number 768K0013-9H, Los Alamos National Laboratory (LANL), 1994.

[30] J. A. Shercliff, *A Textbook of Magnetohydrodynamics.* Pergamon Press Ltd., 1965.

[31] J. Robert E. Peterkin and L. D. Merkle, "Two-dimensional simulations of repetitive pulsed laser interactions with solid targets in air," in *IEEE International Conference on Plasma Science*, 1998.

[32] N. Kubota and I. Aoki, "Burning rate characterization of GAP/HMX energetic composite materials," *Propellants, Explosives, Pyrotechnics*, vol. 25, pp. 168–171, 2000.

[33] J. E. Sinko, N. B. Dhote, J. S. Lassiter, and D. A. Gregory, "Conical nozzles for pulsed laser propulsion," in *Proceedings of SPIE Vol. 7005* (C. R. Phipps, ed.), 2008.

[34] J. E. Sinko and D. A. Gregory, "Critical fluence effects in laser propulsion," in *Proceedings of SPIE Vol. 7005* (C. R. Phipps, ed.), 2008.

[35] M. C. Louwerse, H. V. Jansen, M. N. W. Groenendijk, and M. C. Elwenspoek, "Nozzle fabrication for micropropulsion of a microsatellite," *J. Micromech. Microeng.*, vol. 19, 2009.

[36] J. T. Cassibry, "Theoretical performance of an MHD nozzle using super-alfvenic detachment," in *42nd AIAA/ASME/SAE/ASEE Joint Propulsion Conference & Exhibit*, 2006.

Vita

Richard Joel Thompson was born and raised in North Carolina. He was awarded a Bachelor's of Science degree in physics from Lipscomb University in Nashville, Tennessee. He sought further studies at the University of Tennessee Space Institute in Tullahoma, where he is currently being awarded his Master's of Science degree in mechanical engineering. Joel intends to pursue a doctorate degree to further his education in physics and engineering. His professional interests center around theoretical and computational plasma physics.